EUROPEAN ORGANIZATION FOR NUCLEAR RESEARCH

CERN-EP/87-72
April 9th,1987

MULTIPLE IONIZATION OF He, Ne, AND Ar BY FAST PROTONS AND ANTIPROTONS

L.H. Andersen, P. Hvelplund, H. Knudsen, S.P. Møller,
and A.H. Sørensen
Institute of Physics, University of Aarhus
DK-8000 Aarhus C, Denmark

K. Elsener, K-G. Rensfelt, and E. Uggerhøj
CERN, CH-1211 Geneva 23, Switzerland

PACS No.: 34.50Fa,34.80Dp

(Submitted to Physics Rev.A)

ABSTRACT

Single and multiple ionization of He, Ne and Ar has been studied experimentally by impact of fast protons and antiprotons. The single-ionization cross sections obtained with protons and antiprotons are found to be the same. The double-ionization cross sections obtained with antiprotons, however, are much larger than those obtained with protons at equal velocity. This difference is found for all three gases but the effect is largest for He and Ne, where the difference is about a factor of two at 1MeV/amu. The difference is discussed in terms of interference between two collision mechanisms which both result in double electron escape. Experimental information on the magnitude of the interference term is obtained by inclusion of double-ionization data, partly obtained in this work, for fast electron and alpha-particle impact. For triple ionization of Ne, we also find that antiprotons yield much larger cross sections than protons do. Identical cross sections, however, are found for triple ionization of Ar with protons and antiprotons. This is believed to be due to the fact that triple ionization of Ar is mainly a consequence of a single vacancy produced in an inner shell followed by electronic rearrangement. This observation supports the interpretation that the observed charge effect is due to an interference effect in the outermost shell.

1. INTRODUCTION

In the field of atomic collisions, one has exact knowledge about the forces of interaction between the two nuclei and their attendant electrons. Thus, in principle, any collision process should be managable to the atomic physics theorist. However, even the simplest collision processes constitute a considerable challenge due to the complex dynamics of systems of more than two particles. Today, one of the main goals for atomic physicists is to find appropriate approximations for the many-body problems encountered in atomic collisions. Such solutions are of fundamental interest and important for the understanding of complex systems in nature.

One of the basic processes in atomic collision physics is ionization. Studies of single ionization have been carried out extensively, both theoretically and experimentally, and this process is reasonably well understood especially at high impact velocity where the collision essentially is a two-body process. In particular, the cross section for single ionization scales as q^2, where qe is the charge of the projectile and e the elementary charge.[1]

With the establishment of low energy (~5MeV) antiproton beams at CERN, one has a unique opportunity to test charge scaling for atomic collisions through a comparison between cross sections obtained with protons and antiprotons. Such a comparison constitutes an excellent basis for exploration of charge scalings since protons and antiprotons, with respect to atomic collision processes, only differ by the different sign of the charge. Alternatively, cross sections obtained with electrons and protons can be compared. However, the very different masses make the comparison ambiguous, especially at lower velocities.

At high impact velocity, compared to the orbiting electron velocity, the first Born approximation generally provides a convenient framework for the treatment of single ionization and hence this process is well understood. The situation for multiple ionization is considerably less clarified. Even at high projectile velocities, where the projectile interaction may be treated as a perturbation, proper calculations are very scarce. This is closely connected to the fact that the independent electron model often fails in the description of multi-electron transitions.[3,4] Since in ion-atom collisions most ejected electrons move with relatively little velocity, compared to their original orbital velocity, interactions between electrons are often important in multiple ionization processes. Thus, higher order terms in the Born expansion must be considered. In the present work, we focus on possible quantum mechanical interferences between the various collision amplitudes in the Born expansion for double ionization. Similar effects are observed in electron capture processes at high velocity[5,6].

At lower velocity, ionization processes become more complicated due to a number of effects. For example, for positive ion impact, electron capture contributes to ionization. Moreover, for ionization processes of inner shells of atoms, deviations from the q^2 scaling may occur due to the interaction between the incoming projectile and the target nucleus, and due to changes in the binding of the target electrons due to the presence of the charged projectile.[7]

In a recent publication[8] we reported on single- and double-ionization of He by fast protons and antiprotons. In the present work, we find that protons and antiprotons yield essentially identical cross sections for single ionization. Due to special experimental circumstances, this was not observed in the previous publication.[8] Further, the double-ionization data obtained for He[8] are slightly changed. Here, we include data obtained with the heavier targets Ne and Ar. With these gases the ionization process may be accompanied by Auger processes and shake off when electrons are ejected from

the inner shells of the atom and, accordingly, Ne and Ar constitute a more complicated target than He. Especially for Ar, L-shell ionization is found to be important for the production of doubly and triply charged ions.

For He, we observed a large difference between the double-ionization cross section obtained with protons and antiprotons.[8] It was found that the antiprotons resulted in double-ionization cross sections, which were twice as large as those produced by protons in the energy range 0.5MeV to ~4MeV. We find similar effects for multiple ionization of Ne and Ar, except when the final ionization stage is reached as a consequence of single-vacancy production in inner shells.

Ionization is one of the main processes by which a projectile penetrating matter looses energy. Since multiple ionization is associated with large energy loss, the observed deviation from a q^2 scaling for multiple ionization becomes relevant for the so-called Barkas effect, which is normally defined as departures from the q^2 behaviour of the Bethe stopping power formula. We will discuss the importance of the present results to the Barkas effect.

Throughout this work the notation σ^{Q+},Q=1,2,3 will be used for the total cross section for production of target ions of charge state Q+. It has become customary for multiple ionization to present the data in terms of the ratio between the multiple-ionization and the single-ionization cross sections. We use the notation $R^{(2)}=\sigma^{2+}/\sigma^{+}$ and $R^{(3)}=\sigma^{3+}/\sigma^{+}$.

2. EXPERIMENTAL TECHNIQUE

The apparatus used in the present experiment was designed to fit into the special experimental conditions encountered at CERN. Here, the antiprotons were extracted from the Low-Energy-Antiproton-Ring (LEAR). The beam was extracted at 105.5MeV/c, which corresponds to a kinetic energy of 5.91MeV.

The beam passed through a 110μ Be window, which closed the LEAR vacuum system. The antiprotons then passed through 16 mm atmospheric air and, finally, entered into our experimental arrangement through a 23μ mylar foil. At this point, the energy of the antiprotons were 4.1MeV, which was the maximum kinetic energy used for antiprotons in this work. In order to obtain antiprotons at a lower energy, thin Al foils were placed between the two vacuum systems. We used an annular scintillator located at the entrance to the interaction region to steer the beam through the experimental arrangement (see Fig. 1). Typical p^--beam intensities were between 2 10^4/sec and 10^5/sec.

Since the main purpose of the present work is to compare data for proton and antiproton impact, we established experimental conditions at the EN-tandem accelerator in Arhus, which were similar to those at CERN. That is, protons were accelerated to an energy of 5.91MeV and, subsequently, passed through the same sequence of foils and windows that were used to slow down the antiprotons.

In addition, we have measured relative cross sections with bunched p^+ and He^{2+} beams from the EN-tandem accelerator. The energy range for these measurements was from 0.1MeV to 10MeV and from 1.36MeV to 18MeV, respectively. In these cases, the target vacuum system was linked together with the accelerator vacuum system and no foils nor windows were used. Moreover, similar data have been obtained with 1.5keV to 13keV electrons.

To measure the yield of the various charge states of the target ions created through collisions with the projectiles we used a time-of-flight technique. The target arrangement is shown schematically in Fig. 1. The target gas was located between two parallel condenser plates. Target ions created between the plates were accelerated by an electric field of 800 V/cm. The ions passed through a high transmission grid, placed on one of the condenser plates and entered into the flight tube. Here, the ions were accelerated and thereby focussed by additional -3500 Volts. Finally, they

were recorded by a ceramic channeltron detector the cone of which was biased at -3900 Volts. The time-of-flight system was designed to give ions of a specific charge approximately the same flight time, regardless of the position of creation in the reaction region.

Different techniques were used to provide the information about the time-of-flight of the recoil ions. The DC p^- beam from LEAR and the corresponding p^+ beam from the Arhus accelerator passed through the gas cell and exited through a 1.5μ Al foil. This foil was used in order to avoid a large opening in the gas cell for the relatively broad degraded beam. Subsequently, the beam particles were detected by a 8 cm-diameter scintillator detector located 33 cm behind the gas cell. This detector stopped the beam particles. The STOP pulse to a Time-to-Amplitude Converter was provided by a delayed signal from this scintillator detector. The START pulse was provided by the signal from the channeltron. With the bunched protons and alpha particles, the buncher system provided one of the timing signals. Finally, we used an electron beam in connection with a beam deflection system. In this case, timing pulses from the beam-deflector were used as STOP pulses and pulses from the channeltron were used as START pulses.

Well-resolved peaks, corresponding to different charge states of the target ions, were obtained in the time-of-flight spectra. As an illustrating example, Fig. 2 shows the time-of-flight spectrum for 3.2 MeV p^- on Ne. Charge states of Ne from 1 to 4 are observed. Further, the two Ne isotopes Ne_{20} and Ne_{22} are easily seen. Three peaks occur as a result of interactions with the rest-gas, mainly H^+, OH^+ and H_2O^+. The peak labelled "Prompt", stems from annihilation products created when antiprotons annihilate in the stop scintillator. Some of these products hit and triggered the channeltron and thus coincident START and STOP pulses were generated. Only the "prompt" peak and the H^+, OH^+ and H_2O^+ peaks remained when the target-gas inlet was closed.

On the Ne^+ peak, a tail appeared. This was due to Ne^+ ions undergoing resonant charge exchange with the residual Ne atoms in the flight path from the place of production to the channeltron detector. A similar effect was observed with He and Ar targets. In the data analysis we included this tail as a part of the singly charged peak. In order to eliminate all errors caused by multiple collisions, all yields were extrapolated to zero pressure.

The time-of-flight of target recoil ions was determined by their specific value of M/Q, where M is the mass in amu. If any H_2^+ ions were produced in the target region, they would occur at the same place in the time-of-flight spectrum as He^{2+}. Several checks were made to ensure no contribution from H_2^+. Firstly, with no He gas inlet, no peak appeared at M/Q=2. Secondly, no peak appeared at M/Q=2 with a He_3 inlet. Thirdly, the observed relative amounts of H_2O^+, OH^+ and H^+ were similar to that measured for electrons on water vapor at the same velocity.[9] From the electron data it was found that the amount of H_2^+ produced at these velocities was negligible.

Since we were only able to obtain antiprotons at a fixed energy of 5.91MeV, we inserted degrader foils of different thicknesses to obtain beams of lower energy. Several methods were used to determine the energy of the beam after penetration through the various foils. We calculated the energy by use of proton stopping power values.[10] For the antiprotons these values were corrected to take into account the Barkas effect.[11] This method is expected to yield an accurate energy determination at high energy (>1MeV). At lower energy, where such a calculation may not be accurate, we determined the energy of the antiprotons by measuring the position of the "prompt" peak in the time-of-flight spectrum (see Fig. 2). In Figure 3 is shown $\sqrt{M/Q}$ as a function of flight time for 0.5MeV p^- on Ne. As expected, $\sqrt{M/Q}$ is a linear function of the flight time. Let ΔT be the shift of the "prompt" peak with respect to the straight line. Then ΔT is equal to the flight time of the

projectile from the gas cell to the stop scintillator plus the flight time of the annihilation products from the stop detector to the channeltron. In the following, the annihilation products are assumed to travel with the speed of light. By measuring ΔT, one has thus a direct measure for the speed of the projectile. This method introduced little uncertainty on the energy determination below 1MeV. At higher energies, the uncertainty in the determination of the straight line, shown in Fig. 3, introduced a relatively large uncertainty in the determination of ΔT, which was smaller here. Within the uncertainty, the method, however, predicted energies which were consistent with the calculated values. We estimate the overall uncertainty on the determination of the antiproton energy to be about 100keV at 0.5 MeV and 200keV at all other energies.

The numerical analysis of the data proceeded as follows. Let N^{Q+} be the measured number of recoil ions at charge state Q, N_0 the measured number of beam particles, P the pressure in the gas cell measured in mtorr, and L the length of the collection region in cm; then the cross section for production of target ions of charge Q+ is

$$\sigma^{Q+} = \frac{\varepsilon_0}{\varepsilon^{Q+}} \lim_{P \to 0} \left(\frac{N^{Q+}}{N_0 P} \right) \frac{1}{L \; 3.29 \; 10^{13}} \; [cm^2] \qquad (1)$$

where ε_0 is a normalization constant and ε^{Q+} is the channeltron detection efficiency to detect ions of charge Q+ and energy 3.9Q keV.

For the purpose of normalization, we used the recommended electron production cross section of Rudd et al.[12]

$$\sigma_e = \sum_Q Q \, \sigma^{Q+} = \sigma^+ \left(1 + 2 \frac{\sigma^{2+}}{\sigma^+} + 3 \frac{\sigma^{3+}}{\sigma^+} + \ldots.\right) \qquad (2)$$

By using our measured ratios σ^{2+}/σ^+ and σ^{3+}/σ^+ (see below) and by neglecting other terms, we were able to extract the cross sections for single ionization. ε_0 was found by comparing our results for σ^+ for 4.4 MeV p^+ on

He with those obtained from the recommended values of Rudd et al. In doing so, we set ε^+ for He equal to one. ε^+ for Ne, Ar and Xe was then found through normalization to the single ionization cross sections obtained from Rudd et al. for 4.4 MeV protons on these gases. Figure 4 shows the resulting ε^+ as a function of impact velocity of the recoil ions on the detector. From this curve we also found ε^{Q+}, $Q>1$, since the detection efficiency is a function of impact velocity only independent of the incident charge.[13]

The present apparatus was constructed with a large opening between the collision region and the time-of-flight tube. The reason for this was the large spatial extension of the degraded beams. As a consequence, the pressure was not uniform in the collision region. This influenced the absolute cross sections measured with degraded beams. The relative cross sections, however, were not influenced by this effect.

The relative ionization cross sections were obtained from

$$R^{(Q)} = \frac{\sigma^{Q+}}{\sigma^+} = \frac{\varepsilon^+}{\varepsilon^{Q+}} \lim_{P\to 0} \left\{ \frac{N^{Q+}}{N^+} \right\} . \qquad (3)$$

Thus, N^{Q+}/N^+ was measured as a function of pressure. At low pressures (below ~5mtorr), we found a linear dependence on the pressure. Since we only had a very limited amount of antiprotons, we did not measure the pressure dependence of N^{Q+}/N^+ at all energy/target combinations with antiprotons. Where the pressure dependence for p^- was measured, it exhibited essentially the same pressure dependence as that obtained with protons.

3. RESULTS AND DISCUSSION

3.1 Single Ionization

The main purpose of the present paper is to investigate double and multiple ionization processes and, in particular, the effect on such processes of the sign of the charge of the projectile. The work was stimulated by the unexplained e^{-}-p^{+} difference in double-ionization of He, first noticed by Pucket and Martin[14] and later emphasized by Haugen et al.[15]

At the same incident velocity (1-2MeV/amu), the single-ionization cross sections for electrons and protons were equal as expected. At lower velocities, the presence of electron capture for protons and the appearance of the energy threshold for electrons result in different cross sections for electrons and protons.

At sufficiently high impact velocity the process of single ionization is essentially a two-body process. In this case the first Born approximation constitutes a consistent first-order perturbation theory for ionization. This is so because the ionized electron is left far behind the fast moving projectile, the potential of which makes up the perturbation.[16] This is in contrast to the process of electron capture, where the released electron interacts with the projectile to infinity order. Inokuti[1] has given an excellent review on the matter of inelastic collisions between fast charged particles and atoms within the context of the first Born approximation. Here, the cross section for single ionization is expected to vary as $q^2 \ln(V)/V^2$, where V is the projectile velocity. That is, the cross section is independent of the sign of the charge of the incident particle. Several calculations of ionization within the first Born approximation exist. We refer to the calculations of Bell and Kingston,[17] and Gillespie[18] for He and to that of E.J. McGuire[19] for Ne and Ar targets.

Apart from the effect of electron capture at low energy, there exists a number of other effects at low energy, which can cause deviations from the q^2 scaling predicted by the first Born approximation. This has been discussed by Brandt and Basbas[7] and by Martir and coworkers.[20]

The main result obtained for single ionization in the present work is that within our experimental uncertainties (~10%) the cross sections for proton and antiproton impact are the same. This is as expected on the basis of the first Born approximation. Higher-order effects, as those mentioned above, are not observed. Such effects are generally more pronounced in inner shell ionization processes, where the projectile experiences close encounters with the target nucleus.[7] Single ionization for the present collision systems is dominated by outer shell ionization.[21,22]

3.2 Double ionization

In the last 20 years there has been interest in the problem of double ionization of atoms by photons, electrons and protons. Today, the dynamics of this process still constitutes a challenge to physicists. As pointed out by Byron and Joachain,[3] this is closely related to the fact that, unlike single ionization which can be satisfactorily described within the independent electron model, the process of double ionization depends sensitively on electron correlation effects. Generally, electron correlations are of greatest importance for electrons moving in the field of a low effective nuclear charge, since then the mutual electronic interaction is most important. Thus, systems such as H^- and He are very appropriate for studies of correlation effects.

Single ionization by photon impact at high energy normally results in ejection of one fast electron. Dynamic correlation between the active electron and other target electrons is then insignificant. This situation is described by the sudden approximation.[23] In this approximation, a sudden change in the effective nuclear charge appears. Due to initial-state

correlations, the subsequent electronic relaxation may lead to additional ionization. This process is called shake-off in the sudden approximation and is valid when the first electron is ejected with high velocity. Such a situation is encountered with high energy photon impact[24] and via electron capture to fast positive projectile ions.[25,26] In these cases, the shake-off process is independent of the initial ionization mode and the ratio between the double- and the single-ionization cross sections is a constant.

Shake-off in the sudden approximation describes multiple ionization within the first Born approximation.[3,27] Hence, double ionization may result from one projectile-electron interaction. It should be emphasized that the first Born approximation is only well suited to describe the ionization process when i) the projectile interacts only once with one target electron and ii) the ejected electron leaves the target without further interaction with other target electrons. When one or both criteria fail to apply, higher order Born terms are needed in the Born expansion and multiple ionization cannot be described by shake-off alone.

In ion-atom collisions, generally the ejected electrons leave the atom rather slowly and, consequently, the sudden approximation is not applicable. This is closely connected to the fact that the Coulomb interaction can be described as an exchange of virtual photons, most of which have rather low energy.[1,28] Since the ejected electrons generally are not as fast for charged particle impact as for high energy photon impact and since the final rearrangement process is very sensitive to final state correlations,[3] the particle- and photon-impact rearrangement processes may not be identical. This is indeed the case when the initial ionization process takes place in the same shell as the subsequent rearrangement process, which is the case for He. In this situation, where two or more electrons are removed from the same shell, electron correlations are particularly important.[29] In contrast, ionization of inner shells with shake-off from outer shells seems to be less dependent on correlations.[30] This was emphasized by Stolterfoht et al.,[31]

who showed that after K-shell ionization of Ne, the same amount of shake-off from the L-shell was found for high energy photon, electron and proton impact. Thus, one must distinguish between shake-off from the same shell and from different shells.

In ion-atom collisions, an ejected electron may collide with a second electron, resulting in double ionization. We call this two-step process, which involves only one projectile-target-electron encounter, TS-1.[8] This second Born-type process remains important even at high impact energies since the recoil-velocity of the primary electron is nearly independent of incident ion energy.[28] For lower projectile velocities the projectile may collide with two target electrons and thus result in double ionization. This two-step process,[8,21,22,27,32,33] which we call TS-2, is also a second Born-type process. The importance of TS-2 is, however, vanishing at high projectile velocity.

3.3 Helium

The obtained ratio $R^{(2)}=\sigma^{2+}/\sigma^{+}$ is in Fig. 5 presented as a function of impact energy per mass unit (MeV/amu) for electrons, protons and antiprotons on He. Since our first report on the antiproton results,[8] we have continued with extra proton measurements. Thus, we obtained more reliable extrapolations to zero pressure of N^{2+}/N^{+}, also for antiproton impact. Further, the LEAR Be-window turned out to be ~110μ instead of ~100μ, which was assumed initially. For these reasons, the antiproton data are slightly changed as compared to those reported previously.[8] In Table I are listed our experimentally obtained values of $R^{(2)}$ for p^{+}, p^{-}, e^{-} and He^{2+} on He. As is seen from Fig. 5, our data are generally in good agreement with the results from other experimental works.

It has been an open question whether the difference in double ionization of He with e^- and p^+ impact above 1MeV/amu is due to the different masses or whether it is caused by the different charge of the projectiles.[27,40] Our results with antiprotons from LEAR clearly demonstrate that the difference is a charge effect. The difference for p^+ and p^- is about a factor of two between 0.5MeV/amu and 5MeV/amu. The data indicate that the difference in $R^{(2)}$ disappears at about 50MeV/amu, where the data for e^- and p^+ seems to merge.

When E(MeV/amu) is below ~5, the data for e^- and p^- impact yield different ratios $R^{(2)}$. Most of this difference is caused by different double-ionization cross sections, since the single-ionization cross sections are identical except at very low velocity. The rapid fall-off in $R^{(2)}$ is attributed to the finite threshold energy for double ionization, which for He is 79eV, corresponding to 0.144MeV/amu. It is noted that the data obtained with electrons and antiprotons merge at about 5MeV/amu. Evidently, the energy threshold at 79 eV influences the dynamics of the double-ionization process for electrons, even at an energy in the excess of 2keV. $R^{(2)}$ and $R^{(3)}$ for Ne and Ar also vanish at low e^- impact energy. Since we do not focus on threshold effects in the present work and for the sake of clarity, we only show e^--data for E(MeV/amu)>5 in the remaining figures.

In Fig. 5 we have included the value of $R^{(2)}$ obtained with 40 MeV electrons.[37] The numerical value obtained by these relativistic electrons is about the same as that obtained at much lower energy, indicating that $R^{(2)}$ reaches a value which is nearly energy independent at sufficiently high energy. Later, the energy dependence of $R^{(2)}$ at relativistic energies will be discussed in more detail.

For proton impact, $R^{(2)}$ increases rapidly at low energy (<0.5MeV/amu) due to the increasing importance of electron capture[34] and to the dominance of two-step collisions with the projectile (TS-2). In the Born approximation TS-2 leads to a value of $R^{(2)}$, which is proportional to $q^2(V^2 \ln V)^{-1}$.[27] For

antiprotons there is no charge transfer and the raise is solely caused by TS-2.

It is important to note that the data for charged particle impact yields a value of $R^{(2)}$ which is about $2.5\ 10^{-3}$ for the highest velocities investigated. The value of $R^{(2)}$ for impact of high energy photons is about one order of magnitude larger.[29] There may be two reasons for this difference: First,as discussed, the sudden approximation does not apply for high energy ion impact, that is, dynamical correlations are important. This may cause the electronic relaxation to take place more adiabatically. Second, for ion impact, generally, less energy is transferred to the target electrons, which, in turn, gives a strongly reduced phase space for double ionization.

3.4 Interference Effects

It was McGuire,[27] who first suggested the e^{-}-p^{+} difference to be a charge effect rather than a mass effect. McGuire suggested this difference to be due to an interference between TS-2 and the shake-off process. A coherent addition of the probability amplitudes for the two mechanisms might result in an interference term in σ^{2+}, which is proportional to q^3.

In the dipole approximation, the final state of the TS-2 process is of (pp) symmetry and the shake-off process yields (sp) symmetry, provided that the initial target state is an s-state. Thus, an interference may not be possible.[41] It has been emphasized,[42] however, that in the present velocity region the transitions are not pure dipole-like and that the ground state of He has an appreciable amount of p-character due to electronic correlations.

It has also been suggested that the large difference in the double ionization cross section of He by positive and negative charged particles might be due to an interference between the two second Born mechanisms TS-1 and TS-2.[43] In the present velocity range their amplitudes are comparable.[44] We shall discuss this in more detail shortly.

In the shake-off and the TS-1 process, the projectile interacts only with one of the target electrons through the perturbation $Q_i \equiv -qe^2/r$, whereas the second electron is ejected as a result of electron-electron interaction. The total transition amplitude for these proceses may therefore be written as

$$\breve{a}_I^{fi} = - qa_I^{fi} \quad , \tag{4}$$

where i and f refer to initial and final states and a_I^{fi} is independent of the projectile charge q. The transition amplitude for the TS-2 process, where the projectile interacts with both target electrons, may equivalently be written as

$$\breve{a}_{II}^{fi} = q^2 \quad a_{II}^{fi} \quad . \tag{5}$$

where a_{II}^{fi} is independent of q.

At high projectile velocities, where electron capture may be neglected, the cross section for double ionization is given by the sum of Eqs. (4) and (5), i.e., the cross section attains the value

$$\begin{aligned} \sigma^{2+} &= \sum_f |\breve{a}_I^{fi} + \breve{a}_{II}^{fi}|^2 \\ &= q^2 \sum_f |a_I^{fi}|^2 + q^4 \sum_f |a_{II}^{fi}|^2 - q^3 \sum_f (|a_I^{fi} a_{II}^{fi*} + a_I^{fi*} a_{II}^{fi}) \quad (6) \\ &= q^2 \sigma_I + q^4 \sigma_{II} - q^3 2\sigma_{int} \quad , \end{aligned}$$

where σ_I and σ_{II} are the cross sections for double ionization as a result of one and two interactions with the projectile, respectively. σ_{int} is the contribution due to interferences between the two processes.

Experimentally, $R^{(2)}$ has been measured with q=+1 (protons), q=-1 (antiprotons, electrons) and q=2 (alpha particles). Under the assumption that $\sigma^+(p^+)=\sigma^+(p^-)$ and $\sigma^+(He^{2+})=4\ \sigma^+(p^+)$, which are valid in the energy range >1MeV/amu to be considered in the following, we obtain from Eq. (6)

$$R_I \equiv \sigma_I/\sigma^+(p^+) = R^{(2)}_{p^+} + \frac{1}{3} R^{(2)}_{p^-} - \frac{1}{3} R^{(2)}_{He^{2+}} \quad (7)$$

$$R_{II} \equiv \sigma_{II}/\sigma^+(p^+) = -\frac{1}{2} R^{(2)}_{p^+} + \frac{1}{6} R^{(2)}_{p^-} + \frac{1}{3} R^{(2)}_{He^{2+}} \quad (8)$$

$$R_{int} \equiv \sigma_{int}/\sigma^+(p^+) = \frac{1}{4} (R^{(2)}_{p^-} - R^{(2)}_{p^+}) \ . \quad (9)$$

In order to determine R_I, R_{II} and R_{int}, we have made smooth curve-fits to the experimental data for protons, antiprotons (and high energy electrons), and alpha particles (see Fig. 6). We then calculated R_I, R_{II} and R_{int} from Eqs. (7)-(9) using values of $R^{(2)}$ read from these curves. The result of this approach is shown in Fig. 7. Evidently, R_I turns out to be nearly energy independent, in agreement with the physical interpretation that σ_I (like σ^+) stems from a single interaction with the projectile. Further, R_{II} is essentially proportional to 1/E. This is in agreement with the interpretation of σ_{II} being due to double collisions with the projectile (TS-2). McGuire[27] applied the first Born approximation within the independent electron model and found that $\sigma_{II} \propto 1/E^2$. If we neglect the logarithmic term in the energy dependence of σ^+, then $R_{II}=\sigma_{II}/\sigma^+ \propto 1/E$.

The important new information is contained in R_{int}. The data displayed in Fig. 7 contains the experimental information about the interference between the two amplitudes $\breve{a}^{fi}_I$ and $\breve{a}^{fi}_{II}$. Below, the subject of interference will be discussed in more detail. Here, we shall only emphasize that the data shown in Fig. 7 clearly support the idea that the charge effect in double ionization is due to an interference effect. Note also that the velocity dependence of R_{int} is approximately V^{-1}, as expected from the velocity dependences of σ_I and σ_{II}.

Recently, an ab initio calculation of the double ionization of helium by protons and antiprotons was presented.[45] The time dependent Schrödinger equation was solved using the so-called forced impulse method and s and p pseudo-states only. The calculation predicts a difference in $R^{(2)}$ for p^+ and p^- impact which has qualitatively the right behaviour. The calculation

gives, however, a value of $R^{(2)}$ being ~35% too low as compared to the experimental proton data. Further, the calculated difference between protons and antiprotons is only about half of that observed experimentally between about 1 to 10MeV/amu. The lack of agreement between the calculation and experimental data was attributed[45] to the absence of d-states in the single-particle basis.

The difference has also been attributed to a different distortion of the target electron wave function with positive and negative projectiles.[46] The distortion was related to the presence of electronic correlation in the He ground state. As a consequence, in the two-step process (TS-2) the collision between the second electron and the projectile was associated with a shift in impact parameter of the order of one atomic radius independent of the incident projectile energy. Clearly, such a treatment may be valid at very low velocity but not at high velocities since here the time interval between two successive collisions between the electrons and the projectile is very small. Thus, we believe that such correlation-sensitive polarization effects may be of significance at low velocity but not at high velocities considered in the present experiment. Further, the model predicts little p^+/p^- difference for the heavier targets Ne and Ar, in contrast to the experimental observations for these targets, as discussed later.

3.5 Estimates of the contributions to σ^{2+}

The extensive numerical work performed by Reading and Ford[45] does not give a transparent explanation for the observed variations of $R^{(2)}$ with V and q. In the following, let us therefore consider the various double-ionization mechanisms involved and through some rough estimates try to produce values for the contributions to σ^{2+}, in particular σ_I and σ_{II}. For σ_{int} we shall give no numbers but only discuss how the experimentally observed values seem 'reasonable'.

Our model is the Weizsäcker-Williams scheme of virtual quanta.[47,48] We divide collisions into close and distant encounters, the cross section splits correspondingly

$$\sigma = \sigma_c + \sigma_d \quad . \tag{10}$$

The distant collision contribution is computed by means of the vitual photon method. Here, the basic idea is to replace the perturbing fields of the swift particle by an equivalent pulse of electromagnetic radiation and, then, determine the interaction between projectile and target through known cross sections, σ_γ, for photon interaction. As a result, σ_d is given as

$$\sigma_d = \int_I^\infty d(\hbar\omega)\, \frac{dN}{d\hbar\omega}\, \sigma_\gamma(\omega) \quad , \tag{11}$$

where I denotes the threshold energy of the considered process (single or double ionization). The intensity of virtual quanta of frequency ω is obtained according to the relation[48]

$$\frac{dN}{d\hbar\omega} = q^2\, \frac{2}{\pi}\, \alpha\, (\frac{c}{V})^2\, \frac{1}{\hbar\omega}\, \left[\ln\, (\frac{1.123V}{\omega d}\, \gamma) - \frac{1}{2}\, (\frac{V}{c})^2\right] \quad , \tag{12}$$

where d denotes the dividing distance which separates distant from close collisions and $\alpha = e^2/\hbar c$ is the fine-structure constant. The quantity $\gamma \equiv (1-(V/c)^2)^{-1/2}$ is only of interest at relativistic energies. In case the argument of the logarithm approaches 1, the full expression for the intensity,[48] as defined by the modified Bessel functions K_0 and K_1, should be used rather than the asymptotic relation (12). However, in our cases we may stick to the latter, corrections being of order $(\omega d/V)^2$. It is worthwhile noting that through the construction (11-12) the distant collision contribution to any ionization process scales with projectile charge and velocity as $(q/V)^2 \ln V$.

For single ionization of helium we use the photo cross section given by Lowry et al.[49] which we fit as

$$\sigma_\gamma^+[\text{Mbarn}] = -4.92x^{-3} + 17.3x^{-2} - 5.29x^{-1} + 1.21, \quad 1 \leq x \leq 2.5$$
$$\sigma_\gamma^+[\text{Mbarn}] = \left(\frac{73\text{eV}}{xI^+}\right)^{2.6}, \quad 2.5 < x, \tag{13}$$

where $x=\hbar\omega/I^+$. The main contribution to the integral (11) derives from the region near the threshold $I^+=24.6$eV where our fit reproduces the tabulated cross section to within a few per cent. For double ionization we need values of σ_γ near the double ionization threshold $I^{2+}=79.0$eV. Both the experimental and theoretical information is scarce here; we have made the following fit which reproduces the 'recommended' value of the ratio $\sigma_\gamma^{2+}/\sigma_\gamma^+$ (Ref. 50),

$$\frac{\sigma_\gamma^{2+}}{\sigma_\gamma^+} \simeq 4.6 \ 10^{-2} \left(1 - \left(\frac{I^{2+}}{\hbar\omega}\right)^3\right) . \tag{14}$$

Near I^{2+}, the fit should probably not be trusted better than to within 10-20%. On the other hand, for $\hbar\omega \gg I^+$ the high-energy fit (13) to σ_γ^+ is accurate to within a few per cent.

The minimal impact parameter for distant collisions, d, appears underneath a logarithm, Eq. (12), and the exact choice is not very important. Following Williams,[47] we use $d=\hbar/\sqrt{2mI}$ which quantity is of the order of the radius of the electronical orbit. For close collisions, the momentum transfer to the target electrons attains values $>\hbar/d$. This leads to an energy transfer in excess of the excitation energy, $T>I$, with the above choice for d. Consequently, the contribution σ_c essentially may be obtained from the differential cross section $d\sigma/dT$ for collisions between free particles as

$$\sigma_c = \int_I^{T_{max}} dT \, \frac{d\sigma(T)}{dT} \quad , \tag{15}$$

where the maximum energy transfer is determined by the kinematics.

At non-relativistic energies the differential cross section for scattering on a free electron of mass m (assumed at rest) is given by the Thompson expression,

$$\frac{d\sigma}{dT} = q^2 \, \frac{2\pi e^4}{mV^2} \, \frac{1}{T^2} \quad . \tag{16}$$

For heavy projectiles as well as for swift electrons of energy exceeding I by an order of magnitude or more we may shift the upper limit of integration in Eq. (15) to infinity. For single ionization we then get upon insertion of Eq. (16) into Eq. (15) for the close collision contribution in helium

$$\sigma_c^+ = 3.89 \;\; 10^{-16} \mathrm{cm}^2 \;\; q^2 \left(\frac{v_0}{V}\right)^2 \quad . \tag{17}$$

where $v_0 \equiv \alpha \, c$. A factor of two has been included to account for the fact that a helium atom is dressed with two electrons. By adding the distant collision contribution obtained from Eqs. (11)-(13), where we put $\gamma=1$ and neglect the second term in square brackets in the virtual photon spectrum (velocities of the order of $\sim 10v_0$ are of interest), we arrive for helium at a single-ionization cross section of

$$\begin{aligned} \sigma^+ &= q^2 \left(\frac{v_0}{V}\right)^2 \left[3.72 \, \ln\left(1.04 \, \frac{V}{v_0}\right) + 3.89\right] \;\; 10^{-16} \mathrm{cm}^2 \\ &= 3.72 \;\; 10^{-16} \mathrm{cm}^2 \;\; q^2 \left(\frac{v_0}{V}\right)^2 \ln\left(2.96 \, \frac{V}{v_0}\right) \quad . \end{aligned} \tag{18}$$

At $10v_0$, where more than 2/3 of our cross section derives from distant collisions, the estimate (18) overshoots the recommended values of Rudd et

al. by 25%. This number gives a feeling for the accuracy of the applied method.

Let us now estimate the close-collision contribution to double ionization of helium. We shall simply apply a classical picture - processes like shake-off, corresponding to non-conservation of energy in the intermediate state, are assumed to derive (mainly) from distant collisions. In TS-1, the projectile knocks free an energetic electron which, in turn, on its way out through the atom collides with the second electron. The differential cross section to be inserted in Eq. (15) therefore takes the form

$$\frac{d\sigma}{dT} = \frac{d\sigma_{pe}(T)}{dT} \int_{I^{2+}-I^{+}}^{T-I^{+}} dT' \, \frac{d\sigma_{ee}(T')}{dT'} \langle \int dl |\psi_2|^2 \rangle \, , \qquad (19)$$

the lower limit of integration in Eq. (15) being $I=I^{2+}$. The subscripts pe and ee indicate projectile-electron and electron-electron collisions, respectively. The last factor is the average, over all scattering positions and directions of emission of the first electron, of the integral of the density of the second electron from the scattering point of the first to its escape at infinity. To estimate this average, let us assume simple hydrogen-like orbitals for the electrons in their initial states,

$$|\psi|^2 = \frac{1}{\pi a^3} e^{-2r/a} \, , \qquad a = a_0/Z^* \, , \qquad (20)$$

where Z^* is the effective nuclear charge. The integrand is then independent of the polar and azimuthal angle of the pe scattering point and of the azimuthal component of the emission angle. Only the polar emission angle θ, as measured relative to the axis defined by the nucleus and the pe scattering point, and the radial displacement r of the latter point cause a variation. The sum of the integrated densities for emission angles θ and $\pi-\theta$ equals the single electron density integrated throughout the entire atom along a straight path of impact parameter $b=r\sin\theta$,

$$\varrho(b) \equiv \int_{-\infty}^{\infty} dz |\psi(b,0,z)|^2 = \frac{2b}{\pi a^3} K_1\left(\frac{2b}{a}\right) \quad . \tag{21}$$

The requested average is then defined by the relation

$$\langle \int dl |\psi_2|^2 \rangle = \int_0^{\infty} dr\, r^2\, \frac{4}{a^3}\, e^{-2r/a} \int_0^{\pi/2} d\theta\, \sin\theta\, \frac{2r\sin\theta}{\pi a^3} K_1\left(\frac{2r\sin\theta}{a}\right) \tag{22}$$

where a factor of two again has been included to account for the fact that we have the choice between two target electrons in the first collision. The integral (22) may be computed to yield

$$\langle \int dl |\psi_2|^2 \rangle = \frac{1}{3\pi a^2} \quad . \tag{23}$$

With the Thompson cross section (16), the integral over T,T' in Eqs. (15) and (19) is trivial. By shifting the upper limit of integration to infinity in the pe scattering only, the TS-1 close collision contribution is given by the expression

$$\sigma_{c,TS-1}^{2+} = \left(\frac{q}{V}\right)^2 \frac{2\pi}{3} \frac{e^8}{ma^2} \quad \frac{1}{I^{+2}(I^{2+}-I^{+})} \left\{ \frac{2I^{2+}-I^{+}}{I^{+}} \ln\left(\frac{I^{2+}}{I^{2+}-I^{+}}\right) - 2 \right\} \tag{24}$$

$$= 2.36 \quad 10^{-18}\,\mathrm{cm}^2 \; q^2 \left(\frac{V_0}{V}\right)^2 \quad ,$$

where the last relation follows upon insertion of the numbers I^{+}=24.6eV, I^{2+}=79.0eV and Z*=27/16.

To estimate the cross section for TS-2, consider a projectile moving through the atom on a straight path of impact parameter b. The chance for knocking free first one of the two electrons and, subsequently, the second is

$$\frac{d\sigma^{2+}_{TS-2}}{d\pi b^2} = \sigma(T>I^+)\sigma(T>I^{2+}-I^+)\ \{\int_{-\infty}^{\infty} 2\ dz|\psi(z)|^2 \int_z^{\infty} dz'|\psi(z')|^2$$

$$= \sigma(T>I^+)\sigma(T>I^{2+}-I^+)\varrho^2(b)\ , \tag{25}$$

where $\varrho(b)$ is defined in Eq. (21). The integral over b yields

$$\int d(\pi b^2)\varrho^2(b) = \frac{1}{3\pi a^2}\ , \tag{26}$$

the same number which was also obtained in Eq. (23). Introducing the Thompson cross section, again with $T_{max} \to \infty$, we arrive at a contribution of

$$\sigma^{2+}_{TS-2} = \left(\frac{q}{V}\right)^4 \frac{4\pi}{3} \frac{e^8}{m^2a^2} \frac{1}{I^+} \frac{1}{I^{2+}-I^+}$$

$$= 1.85\ \ 10^{-16}\,cm^2\ q^4 \left(\frac{v_0}{V}\right)^4\ , \tag{27}$$

where the last relation holds for the standard parameters, cf. Eq. (24).

The contribution to double ionization labelled σ_I in Eq. (6) evidently equals the sum of σ_d^{2+} and $\sigma^{2+}_{c,TS-1}$. Computing σ_d^{2+} according to Eqs. (11)-(14), again with the second term in square brackets in Eq. (12) put to zero, we obtain

$$\sigma_I = \left(\frac{v_0}{V}\right)^2 \left[6.7\ \ln(0.53\ \frac{V}{v_0}) + 23.6\right]\ \ 10^{-19}\,cm^2$$

$$= 6.7\ 10^{-19}\,cm^2\ \left(\frac{v_0}{V}\right)^2 \ln(18\ \frac{V}{v_0})\ . \tag{28}$$

At $10v_0$, only 1/3 of σ_I derives from distant collisions. The TS-2 contribution corresponds directly to σ_{II}, i.e.

$$\sigma_{II} = \sigma^{2+}_{TS-2} / q^4 = 1.85 \quad 10^{-16} cm^2 \quad (\frac{v_0}{v})^4 \quad . \qquad (29)$$

Our predictions for $R_{I,II}$, cf. Eqs. (18), (28) and (29), are shown as dashed curves in Fig. 7. Clearly, the agreement between our estimates and the empirical data is very good for R_I. For R_{II}, the agreement is better than 25% above $10v_0$, indeed, already at $20v_0$ differences amount to only 10%. In view of our rough procedure, we could never have hoped to do any better!

In Fig. 6 we displayed a single experimental recording for $R^{(2)}$ at ultrarelativistic impact, $\gamma>>1$. At such energy the single ionization cross section attains the value

$$\sigma^+ = 1.98 \quad 10^{-20} cm^2 \quad q^2 \ln(248\gamma) \qquad (30)$$

with the fit (13). The cross section for double ionization corresponds at high velocities solely to σ_I, which for $\gamma>>1$ is given as

$$\sigma^{2+} = 3.6 \quad 10^{-23} cm^2 \quad q^2 \ln(1470\gamma) \qquad (31)$$

in our model. At ultrarelativistic energies the accuracy of our method is in general much higher than at $\sim 10v_0$. However, our prediction, according to Eqs. (30) and (31), for the 40MeV electron point is ~20% lower than the experimental value. This could very well be due to poor knowledge of $\sigma^{2+}_\gamma / \sigma^+_\gamma$ near I^{2+}, cf. Eq. (14): At ultrarelativistic impact both σ^+ and σ^{2+} are dominated by distant collisions. On the other hand, at $\sim 10v_0$ a 20% correction to σ^{2+}_d would only cause a correction to $R^{(2)}$ of 7%.

We now turn to a discussion of the interference term σ_{int}, introduced in Eq. (6). For the high velocities, $\sim 10v_0$, and the heavy projectiles of concern, the impact parameter b relative to the target nucleus is a well-defined quantity on the scale d. Consequently, only processes occurring at a given value of b may interfere. This immediately implies that we expect the interference in double ionization to set up (mainly) between the two close-

collision contributions, TS-1 and TS-2. Distant collisions do not contribute to σ_{int} since the ionization amplitude here contains solely an a_I-component scaling linearly with projectile charge, cf. the discussion following Eq. (12).

To proceed, consider the second-order matrix element M_2, the norm-square of which defines the transition rate from given initial to final state, $|i\rangle \to |f\rangle$. With two consecutive perturbations Ω and Ω', M_2 takes the form

$$M_2 = \mathcal{P}\int dE_n \varrho(n)\, \frac{\langle f|\Omega'|n\rangle\langle n|\Omega|i\rangle}{E_n - E_i} + i\pi\left[\langle f|\Omega'|n\rangle\langle n|\Omega|i\rangle \varrho(n)\right]_{E_n=E_i} \qquad (32)$$

where $|n\rangle$ denotes an intermediate state of energy E_n populated as a result of the first perturbation. Such states appear with a density $\varrho(n)$. The symbol $\mathcal{P}$ indicates the principal value; the corresponding part of the matrix element is "off the energy shell". On the other hand, the pole term corresponds to energy conservation in the intermediate state ("on the energy shell"). Under the assumption of hydrogen-like 1s wave functions, Eq. (20), for the target electrons in their initial states and plane waves (normalized in a box of volume L^3) for all free particles, the product $\langle f|\Omega'|n\rangle\langle n|\Omega|i\rangle$ of the two first-order matrix elements responsible for TS-2 and TS-1 are, respectively,

$$q^2 e^4 2(8\pi)^3 \frac{a^3}{L^3} (\vec{k}_0 - \vec{k}')^{-2} (\vec{k}' - \vec{k})^{-2} (1+[\vec{k}_0 - \vec{k}' - \vec{k}_1]^2 a^2)^{-2} (1+[\vec{k}' - \vec{k} - \vec{k}_2]^2 a^2)^{-2},$$

$$-qe^4 2(8\pi)^3 \frac{a^3}{L^3} (\vec{k}_0 - \vec{k})^{-2} (\vec{k}_1' - \vec{k}_1)^{-2} (1+[\vec{k}_0 - \vec{k} - \vec{k}_1']^2 a^2)^{-2} (1+[\vec{k}_1' - \vec{k}_1 - \vec{k}_2]^2 a^2)^{-2}. \qquad (33)$$

We have labelled the first liberated electron by index 1, its momentum in the final state is $\hbar\vec{k}_1$, that of the second $\hbar\vec{k}_2$, and $\hbar\vec{k}_0$ and $\hbar\vec{k}$ are the momenta of the projectile before and after the interaction. Primes indicate intermediate states, in TS-2 this is a free projectile wave of momentum $\hbar\vec{k}'$, in TS-1 a free electron wave of momentum $\hbar\vec{k}_1'$.

Since the expressions (33) are real, the principal-value term in Eq. (32) itself is real whereas the pole term is purely imaginary. Consequently, the cross section splits in two,

$$\sigma^{2+} = \sigma^{2+}_{on} + \sigma^{2+}_{off} \quad . \tag{34}$$

From Eq. (33) it is evident that the pole contribution σ_{on} leads to constructive interference for negatively charged projectiles but to destructive for particles of positive charge - in agreement with observations. However, for the principal-value term we cannot argue in any simple way since the energy denominator measuring the difference between initial and intermediate state energies may take any sign.

To estimate the size of the interference effect, it is necessary to find the relative magnitude of the two contributions in Eq. (34) and, in turn, to get an idea of the fraction of the cross section which derives from final states which may be populated by both TS-1 and TS-2. The success of our simple-minded classical estimates hints at a dominance of the pole term for the TS-processes. Therefore, if we take the experimental value of R_{int} and divide by $[R_{II}(R_I - \sigma_d^{2+}/\sigma_d^{+})]^{1/2}$, we may expect to get an idea of the requested fraction. In the velocity region of Fig. 7 we find from the displayed curves with our theoretical estimates for $\sigma_d^{2+}/\sigma_d^{+}$ a slightly varying ratio,

$$0.40 \leq \frac{R_{int}}{[R_{II}(R_I - \sigma_d^{2+}/\sigma_d^{+})]^{1/2}} \leq 0.50 \quad , \tag{35}$$

where the lower limit corresponds to high velocities.

The final question to be answered is now if the values (35) appear reasonable. From the expressions for the matrix elements (33) we see that at each vertex the momentum of the incoming particle tends to be balanced by those of the out-going particles. Deviations are of order $\hbar/a$, which corresponds to the momentum of the electron in the initial state. In consequence, in collisions where both electrons are ejected with high

velocities, $k_i > 1/a$, we essentially have momentum conservation as in collisions with free electrons at rest. For such cases, both electrons in TS-2 are therefore leaving the atom in directions transverse to the projectile path whereas in TS-1 only the first tends to take off transversely, the second may choose any direction. In other words, final states involving two high-energy electrons do not lead to interference. In contrast, with a freedom in momentum within $\hbar/a$, any final state, where both electrons attain momenta $\hbar k_i < \hbar/a$, may be populated via both TS-1 and TS-2. For such states we therefore expect full interference. With the Thompson expression (16), half of the total cross section $\sigma(T>I)$ corresponds to an energy transfer in the interval $I \leq T \leq 2I$, in our picture to an electron leaving the atom with a kinetic energy $\leq I$. The other half stems from final electron states of kinetic energy $\geq I$. Roughly speaking, in double ionization we therefore have 25% contribution from states with full interference, $k_i < 1/a$, and 25% contribution from states with no interference, $k_i > 1/a$. In conclusion, we would expect the ratio tested in Eq. (35) to be in the interval between 0.25 and 0.75 in good agreement with the actual observations.

3.6 Double ionization of Ne and Ar

We now turn to the discussion of double ionization of Ne and Ar. For these targets, double ionization may result from ionization of outer shells as well as from ionization of inner shells. In the latter case, multiple ionization may occur due to Auger processes and shake-off. In the following analysis we assume that, after a single-ionization event from an inner shell, the subsequent electronic relaxation is independent of the incident particle. This has been shown to be a good assumption when the incident energy is not too low, and when photons, electrons and protons are considered.[31] Further, to estimate the role of inner-shell ionization in the production of doubly- and triply-charged ions, we applied the results of

Carlson et al.,[51] who obtained final charge state distributions of atoms after creation of a single hole in a given electronic shell by photon impact.

In Fig. 8 σ^{2+}/σ^{+} for Ne is shown as a function of projectile energy per mass unit (MeV/amu). Shown are results for proton, antiproton and electron impact obtained in the present work together with other proton and electron data. In Table II we present our data (including data obtained with α-particle impact). Apparently, the data are very similar to those obtained with He target, except that for Ne σ^{2+}/σ^{+} is approximately a factor of 10 larger than for He. We attribute this to the larger number of outer-shell electrons in Ne. Between 0.5 MeV/amu and 4 MeV/amu the antiproton data are approximately a factor of two higher than the proton data. Moreover, the antiproton data seems to merge with the electron data at high velocity. We obtain values of $R^{(2)}$ with electron impact, which are slightly higher than those obtained by other groups at equal velocity.[35,36] This may be caused by different estimates of the recoil ion detection efficiency ε^{Q+}. We note that our values seem to be in very good agreement with those obtained at relativistic velocities.[37] The similarity between the He-target and the Ne-target data suggests that the collision mechanisms responsible for double ionization may be identical.

To estimate the contribution from ionization of the K-shell of Ne to double ionization, σ_K^{2+}, we used well-known K-shell ionization cross sections for proton impact[52] and multiplied these cross sections by 0.74, which is the fraction that yields charge state 2+ after one hole being produced in the K-shell.[51] We find that σ_K^{2+} only contributes very little to the double-ionization cross section in the present energy range, in agreement with earlier findings.[21,22] At very high energies (>>10MeV), double ionization of Ne may eventually result from single ionization of the K-shell followed by electronic rearrangement. Thus, in the present discussion of σ^{2+}/σ^{+} for Ne, we need only to consider TS-1, TS-2 and shake-off processses in the

outermost shell.

As for the He-target case, we have determined R_I, R_{II} and R_{int} for Ne from Eqs. (7)-(9) and fits to the experimentally obtained $R^{(2)}$ for impact of q=1 (protons) q=-1 (antiprotons, high energy electrons) and q=2 (α-particles) (see Table II). The result of this approach is displayed in Fig. 9. It is quite evident that for Ne the same conclusions can be made as for He. That is, the difference in $R^{(2)}$ between p^+ and p^- impact may be attributed to a quantum mechanical interference between two different collision amplitudes, which both result in double ionization (see Eqs. (4) and (5)).

The ratio $R^{(2)}$ for the Ar-target is shown in Fig. 10 and listed in Table III. In the table, we include our data obtained with α-particles. From Fig. 10 it is evident that the antiproton data still merge with the electron data at around 5MeV/amu. The difference between data obtained with protons and antiprotons is smaller for Ar than for He and Ne. Moreover, in contrast to that observed for the other targets, the ratio $R^{(2)}$ increases slightly with increasing velocity for E(MeV/amu)>3.

In the present velocity regime ionization of the Ar K-shell is not important.[54] Ionization of the L-shell, on the other hand, must be considered. In Fig. 11 is shown the total double ionization cross section with proton impact together with the contribution to the double-ionization cross section due to single ionization of the L-shell. Cross sections for ionization of the 2s and the 2p orbitals were obtained from Choi et al.[55] The weight factors were taken from the work of Carlson et al.[51] Unlike the situation for Ne, 50% or more of the double ionization cross section of Ar by proton impact between 1 and 5 MeV is due to inner-shell ionization. Since the single-ionization cross section of the L-shell at not too low energies presumably is independent of the sign of the charge of the projectile, the smaller difference between proton and antiproton data is attributed to the presence of inner-shell ionization. The slight increase of the data at high

energy is also attributed to the presence of inner-shell ionization. After subtraction of the large contribution due to inner-shell ionization, it is evident that a pronounced charge effect is also observed for double ionization of the outer shell of Ar.

The experimental data for double ionization of He, Ne and Ar all exhibit a pronounced p^+/p^- difference, which is attributed to ionization of the outermost shells. The charge effect is large for the He target as well as for the heavier targets. This suggests that the p^+/p^- difference is not crucially dependent on static electronic correlation in the initial target state. At any velocity, dynamic correlation or intermediate state correlation is important with charged particle impact since here the first ionized electron moves with relatively low velocity and, consequently, has ample time to interact with other target electrons.

3.7 Triple ionization

Our proton and antiproton data for σ^{3+}/σ^+ in Ne- and Ar-targets are presented in Figs. 12 and 13. In the Ne-target case, a very large charge effect is seen. The effect is even larger than that observed in double ionization. At high velocity, the data for electron, proton and antiproton impact seem to merge as they do for double ionization. For triple ionization this happens at a lower velocity than for double ionization, probably due to the rapidly decreasing cross section for triple collisions. In the Ar-target case, on the other hand, there is no charge effect; antiproton and proton impact result in the same amount of triple ionization. Moreover, $R^{(3)}$ increases with increasing velocity for Ar. As expected, the electron data coincide with the proton/antiproton data at high velocity.

The striking difference between the two targets Ne and Ar is explained in Figs. 14 and 15. For protons on Ar, σ^{3+} can essentially be accounted for in terms of L-shell ionization followed by electronic relaxation. This is not the case for Ne, where an appreciable amount of the triple-ionization

cross section is due to multiple collisions in the outer shell.

We emphasize that at the lowest energy investigated (0.5MeV/amu), the K-shell ionization cross section of Ne may be charge dependent. Due to the Coulomb deflection, the decreased binding effect and the increased speed of the antiproton near the target nucleus, the antiprotons may produce more K-shell holes than the protons do[7] and, thus, result in more doubly- and triply-charged Ne ions. These effects are not important at higher energies.

The fact that the charge effect is observed for target atoms where multiple collisions in the outer shell are important lends support to the idea that at the ion velocities considered here, the charge effect for triple ionization of Ne is due to quantum mechanical interferences between the various amplitudes yielding triple ionization.

3.8 The Barkas effect

The difference in the range of heavy particles of opposite charge under otherwise equal conditions is called the Barkas effect.[56] This classical charge effect represents deviations from the q^2 scaling predicted by Bethe's stopping power formula derived on basis of the first Born approximation. In the past twenty years, there has been considerable interest in such correction terms to the Bethe stopping power formula. In particular, the first term, proportional to q^3, is usually referred to as a polarization effect. Hence, hitherto the Barkas effect is explained as a polarization effect. There has been several attempts to calculate the q^3 correction; the reader is referred to the review of Basbas.[56]

The sign of the Barkas correction term to the Bethe stopping power is such that the range of negatively charged particles is larger than the corresponding range for positively charged particles. The main process by which projectiles lose energy when penetrating matter is ionization. Recalling that double and sometimes triple-ionization cross sections for p^- are larger than the corresponding cross sections obtained with p^+, it is

immediately seen that with the present data, a new contribution to the q^3 correction is introduced. This contribution is of opposite sign compared to that due to polarization effects and has not been considered previously.

In the evaluation of the stopping power, the cross sections are weighted by the energy transfer T. Thus, it is relevant to estimate $\int T d\sigma$. We make the following expansion

$$\int T d\sigma = \int^0 T d\sigma + \int^+ T d\sigma + \int^{2+} T d\sigma + \ldots . \tag{36}$$

where the integral is divided up according to the final ionization stage of the target atom. To estimate the importance of double ionization on the stopping power, we consider the ratio R_s

$$R_s = \frac{I^{2+}\sigma^{2+}}{\int T d\sigma} , \tag{37}$$

where I^{2+} is the energy required to doubly ionize the target. As a particular example, consider 2MeV p^+ on Ne. From the present results and reference 10, we find that R_s is about 2%. Since $\sigma^{2+}(p^-)/\sigma^{2+}(p^+)=1.6$, we obtain an "opposite" Barkas effect, which amounts to 1.2%. This number represents a lower limit since we used I^{2+} as the energy transfer in collisions leading to double ionization, that is, the kinetic energy of the two outgoing electrons have been neglected. This new effect is non-negligible compared to the "normal" Barkas effect[57] of 4.3% in the case considered.

We find that the present effect is negligible for the stopping power of He due to the very small double-ionization cross section. Further, contributions due to triple ionization of Ne and Ar are also small. The effect from double ionization of Ne and Ar is important, however, and cannot be disregarded in any discussion of the Barkas effect.

4. CONCLUSION

In conclusion, it has been found that the single ionization cross section of He, Ne and Ar by p^+ and p^- are, within experimental uncertainties, identical at energies from 0.5MeV to ~5MeV. In the same energy region, the double-ionization cross sections obtained with p^- are about a factor of two larger than those obtained with p^+. The difference has been discussed in terms of interference between two collision mechanisms, one of which corresponds to a single interaction between the projectile and the target and another, which corresponds to two such interactions. By comparison of experimental data obtained with p^+, p^-, e^- and α particles at equal-velocity, the double-ionization cross section has been separated into contributions scaling with projectile charge q as q^2, q^3 and q^4, respectively. Through the construction of a naive model, it has been possible for the He target to reproduce theoretically the q^2 (single projectile interaction) and q^4 (double projectile interaction) terms. Further on, the magnitude and, of course, the sign of the q^3 (interference) term seem reasonable.

For multiple ionization of Ne and Ar, the role of inner-shell ionization has been discussed. Ionization of the Ar-L shell contributes to double as well as triple ionization. In the latter case the entire cross section basically is found to be due to production of L-shell vacancies followed by electronic rearrangement. This, in turn, results in identical triple-ionization cross sections of Ar with p^+ and p^- impact. In contrast, triple ionization of Ne is mainly due to outer-shell ionization. The triple-ionization cross section of Ne by p^- is about a factor of four larger than that obtained by p^+; this p^+/p^- difference is attributed to interference between collision amplitudes leading to triple ionization of the outer shell.

Finally, the present results are shown to be important in the evaluation of the so-called Barkas effect in the stopping power of fast-charged particles.

Acknowledgement

We are much indebted to Jens Lindhard for enlightening discussions and valuable suggestions. The Danish participation in this collaboration was made possible by grants from the Danish Committee for Accelerator Physics.

REFERENCES

1) M. Inokuti, Rev.Mod.Phys. 43 (1971) 297.

2) H.K.Haugen, L.H. Andersen, P. Hvelplund and H. Knudsen, Phys.Rev. A 26 (1982) 1950.

3) F.W. Byron, Jr., and C.J. Joachain, Phys.Rev.Lett. 16 (1966) 1139; F.W. Byron, Jr., and C.J. Joachain, Phys.Rev. 164 (1967) 1.

4) J.H.McGuire in Proc.US-Mexico Joint Symp. on Electron Correlations, Cocoyoc, Mexico (1986).

5) E. Horsdal-Pedersen, C.L. Cocke and M. Stockli, Phys.Rev.Lett. 50 (1983) 1910.

6) J.H.McGuire, P.R. Simony, O.L. Weaver and J. Macek, Phys.Rev. A 26 (1982) 1109.

7) W. Brandt and G. Basbas, Phys.Rev. A 27 (1983) 578.

8) L.H. Andersen, P. Hvelplund, H. Knudsen, S.P. Møller, K. Elsner, K.-G. Rensfelt and E. Uggerhøj, Phys.Rev.Lett. 57 (1986) 2147.

9) J. Schutten, F.J. De Heer, H.R. Moustafa, A.J.H. Boerboom and J. Kistemaker, J.Chem.Phys. 44 (1966) 3924.

10) H.H. Andersen and J.F. Ziegler: The Stopping and Ranges of Ions in Matter, Vol. 3 (Pergamon Press, 1977).

11) J. Lindhard, Nucl.Instr.Methods 132 (1976) 1.

12) M.E. Rudd, Y-K. Kim, D.H. Madison and J.W. Gallagher, Rev.Mod.Phys. 57 (1985) 965.

13) K.H. Krebs, Fortschritte der Physik 16 (1968) 419.

14) L.J. Puckett and D.W. Martin, Phys.Rev. A 1 (1970) 1432.

15) H.K. Haugen, L.H. Andersen, P. Hvelplund and H. Knudsen, Phys.Rev. A 26 (1982) 1962.

16) K. Taulbjerg in Fundamental Processes in Energetic Atomic Collisions, ed. by H.O. Lutz, J.S. Briggs and H. Kleinpopping (Plenum Publ.Co., (1983) 349.

17) K.L. Bell and A.E. Kingston, J.Phys. B 2 (1969) 653.

18) G.H. Gillespie, Phys.Lett. 72A (1979) 329.

19) E.J. McGuire, Phys.Rev. A 3 (1971) 267.

20) M.H. Martir, A.L. Ford, J.F. Reading and R.L. Becker, J.Phys. B 15 (1982) 1729.

21) M. Eckhardt and K-H. Schartner, Z.Phys. A 312 (1983) 321.

22) S.T. Manson, R.D. DuBois and L.H. Toburen, Phys.Rev.Lett. 51 (1983) 1542.

23) T.A. Carlson and M.O. Krause, Phys.Rev. 140 (1965) A1057.

24) T.A. Carlson, W.E. Moddeman and M.O. Krause, Phys.Rev. A 1 (1970) 1406.

25) H. Knudsen, L.H. Andersen, P. Hvelplund, J. Sørensen and D. Ciric, to appear in J.Phys. B Letters (1987).

26) E. Horsdal-Pedersen and L. Larsen, J.Phys. B 12 (1979) 4085.

27) J.H. McGuire, Phys.Rev.Lett. 49 (1982) 1153.

28) J.H. McGuire, J.Phys. B 17 (1984) L779.

29) T.A. Carlson, Phys,Rev. 156 (1967) 142.

30) T.A. Carlson and M.O. Krause, Phys.Rev. 137 (1965) A1655.

31) N. Stolterfoht, H. Gabler and U. Leithäuser, Phys.Lett. 45A (1973) 351.

32) H. Knudsen, L.H. Andersen, P. Hvelplund, G. Astner, H. Cederquist, H. Danared, L. Liljeby and K-G. Rensfelt, J.Phys. B 17 (1984) 3545.

33) A.K. Edwards, R.M. Wood and R.L. Ezell, Phys.Rev. A 32 (1985) 1873.

34) M.B. Shah and H.B. Gilbody, J.Phys. B 18 (1985) 899.

35) B.L. Schram, A.J.H. Boerboom and J. Kistemaker, Physica 32 (1966) 185.

36) P. Nagy, A. Skutlartz and V. Schmidt, J.Phys. B 13 (1980) 1249.

37) A. Müller, W. Groh, U. Kneissl, R. Heil, H. Ströher and E. Salzborn, J.Phys. B 16 (1983) 2039.

38) K. Stephan, H. Helm and T.D. Märk, J.Chem.Phys. 73 (1980) 3763.

39) B. Adamczyk, A.J.H. Boerboom, B.L. Schram and J. Kistemaker, J.Chem.Phys. (1966) 4640.

40) J.F. Reading, Bull.Am.Phys.Soc. 29 (1984) 821; J.F. Reading and L. Ford, submitted to J.Phys. B (1987).

41) A.L. Ford and J.F. Reading, Nucl.Instr.Methods B10/11 (1985) 12.

42) J.H. McGuire, private communication (1986).

43) J. Lindhard and A.H. Sørensen, private communication (1986).

44) M.Gryzinski, Phys.Rev. A 138 (1965) 336.

45) J.F. Reading and A.L. Ford, Phys.Rev.Lett. 58 (1987) 543; J.F. Reading and A.L. Ford, submitted to J.Phys. B.

46) L. Vegh, private communication (1986).

47) E.J. Williams, Mat.Fys.Medd.Dan.Vid.Selsk. 13, No. 4 (1935).

48) J.D. Jackson: Classical Electrodynamics (Wiley, New York, 1975).

49) J.F. Lowry, D.H. Tombonlian and D.L. Ederer, Phys.Rev. 137 (1965) A1054.

50) T. Andersen, private communication.

51) T.A. Carlson, W.E. Hunt and M.O. Krause, Phys.Rev 151 (1966) 41.

52) H. Paul, Nucl.Instr.Methods 169 (1980) 249.

53) B.L. Schram, Physica 32 (1966) 197.

54) L.M. Winters, J.R. Macdonald, M.D. Brown, L.D. Ellsworth and T. Chiao, Phys.Rev. A 7 (1973) 1276.

55) B.H. Choi, E. Merzbacher and G.S. Khandelwal, Atomic Data 5 (1973) 291.

56) G. Basbas, Nucl.Instr.Methods B4 (1984) 227.

57) J.D. Jackson and R.L. McCarthy, Phys.Rev. B6 (1972) 4131.

FIGURE CAPTIONS

Figure 1:

Schematic drawing of the experimental setup used for measurements with degraded p^+ and p^- beams. The dashed lines indicate the beam size (FWHM) for ~4MeV p^-: The numbers show 1) accelerator facility vacuum, 2) time-of-flight tube, 3) channeltron detector, 4) stop detector.

Figure 2:

Time-of-flight spectrum obtained with 3.2MeV p^- on Ne.

Figure 3:

$\sqrt{M/Q}$ as a function of flight time for 0.5MeV p^- on Ne.

Figure 4:

Recoil ion detection efficiency as a function of impact velocity. The data are normalized so that $\varepsilon^+(He)\equiv 1$.

Figure 5:

The ratio $R^{(2)}$ between double- and single-ionization cross sections for p^+, p^- and e^- colliding with He. (■) p^- this work, (●) p^+ this work, (◘) e^- this work, (O) p^+ Refs. 14, 32, 34, (□) e^- Refs. 35-39.

Figure 6:

Smooth curve-fit to experimental data for $R^{(2)}$ for the He target.

Figure 7:

R_I, R_{II} and R_{int} as a function of E (MeV/amu) for the He target. Solid curves represent R_I, R_{II} and R_{int} as obtained from fits to experimental data for protons, antiprotons, high-energy electrons and alpha particles as shown in Fig. 6. The dashed curves result from theoretical estimates, Eqs. (18), (28) and (29).

Figure 8:

The ratio $R^{(2)}$ between double- and single-ionization cross sections for p^+, p^- and e^- colliding with Ne. (■) p^- this work, (●) p^+ this work, (⛁) e^- this work, (O) p^+ Ref. 15, (□) e^- Refs. 35-37.

Figure 9:

R_I, R_{II} and R_{int} as functions of E(MeV/amu) for the Ne target. R_I, R_{II} and R_{int} have been determined from fits to experimental data for protons, antiprotons, high-energy electrons and α-particles.

Figure 10:

The ratio $R^{(2)}$ between double- and single-ionization cross sections for p^+, p^- and e^- colliding with Ar. (■) p^- this work, (●) p^+ this work, (⛁) e^- this work, (O) p^+ Ref. 15, (□) e^- Refs. 36, 37, 53.

Figure 11:

The double-ionization cross section for p^+ on Ar (σ^{2+}) together with the contribution to double ionization due to L-shell ionization σ_L^{2+}. σ^{2+} is obtained from $R^{(2)}$ and σ^+ from Ref. 12 and Eq. (2).

Figure 12:

The ratio $R^{(3)}$ between triple- and single-ionization cross sections for p^+, p^- and e^- colliding with Ne. (■) p^- this work, (●) p^+ this work, (▬) e^- this work, (0) p^+ Ref. 15, (□) e^- Refs. 35-37.

Figure 13:

The ratio $R^{(3)}$ between triple- and single-ionization cross sections for p^+, p^- and e^- colliding with Ar. (■) p^- this work, (●) p^+ this work, (▬) e^- this work, (0) p^+ Ref. 15, (□) e^- Refs. 36, 37, 53.

Figure 14:

The triple-ionization cross section for p^+ on Ne, σ^{3+} is shown together with the contribution to triple ionization due to K-shell ionization σ_K^{3+}. σ^{3+} is obtained from $R^{(3)}$ and σ^+ from Ref. 12 and Eq. (2).

Figure 15:

The triple-ionization cross section for p^+ on Ar, σ^{3+} is shown together with the contribution to triple ionization due to L-shell ionization σ_L^{3+}. σ^{3+} is obtained from $R^{(3)}$ and σ^+ from Ref. 12 and Eq. (2).

TABLE 1.

$R^{(2)}$ for p^+, p^-, e^- and He^{2+} on He obtained in this work.

E(MeV)	Projectile	$R^{(2)}=\sigma^{2+}/\sigma^+$ $[10^{-3}]$
0.10	p^+	17.3 ± 0.30
1.00	-	3.32 ± 0.10
1.20 ± 0.2	-	3.12 ± 0.20
1.90	-	2.80 ± 0.20
2.00	-	2.76 ± 0.06
3.00	-	2.64 ± 0.14
3.20	-	2.50 ± 0.20
4.10	-	2.50 ± 0.15
4.40 ± 0.2	-	2.50 ± 0.10
5.00	-	2.58 ± 0.10
7.00	-	2.51 ± 0.07
10.00	-	2.49 ± 0.10
0.50 ± 0.1	p^-	10.0 ± 0.60
0.90 ± 0.2	-	7.15 ± 0.25
1.90 ± 0.2	-	5.80 ± 0.25
3.20 ± 0.2	-	5.00 ± 0.25
4.10 ± 0.2	-	4.50 ± 0.25
1.5 10^{-3}	e^-	4.22 ± 0.15
2.0 10^{-3}	-	4.20 ± 0.15
3.0 10^{-3}	-	4.10 ± 0.15
4.0 10^{-3}	-	3.67 ± 0.15
5.0 10^{-3}	-	3.47 ± 0.10
7.0 10^{-3}	-	3.34 ± 0.15
9.0 10^{-3}	-	3.29 ± 0.15
11.0 10^{-3}	-	3.13 ± 0.15
13.0 10^{-3}	-	3.00 ± 0.15
1.36	He^{2+}	32.20 ± 0.20
2.00	-	20.95 ± 0.05
2.80	-	14.25 ± 0.10
4.00	-	10.20 ± 0.10
6.00	-	7.05 ± 0.10
9.24	-	5.25 ± 0.05
12.80	-	4.20 ± 0.05
18.00	-	3.65 ± 0.05

TABLE 2

$R^{(2)}$ and $R^{(3)}$ for p^+, p^-, e^- and He^{2+} on Ne obtained in this work.

E(MeV)	Projectile	$R^{(2)}=\sigma^{2+}/\sigma^+$ [10^{-2}]	$R^{(3)}=\sigma^{3+}/\sigma^+$ [10^{-3}]
0.10	p^+	9.69 ± 0.20	6.53 ± 0.20
0.50 ± 0.10	–	3.70 ± 0.30	3.09 ± 0.20
1.00	–	3.42 ± 0.06	1.80 ± 0.36
1.20 ± 0.20	–	2.77 ± 0.20	1.59 ± 0.30
1.90	–	3.10 ± 0.20	2.20 ± 0.30
2.00	–	2.81 ± 0.02	1.93 ± 0.35
3.00	–	2.68 ± 0.04	2.07 ± 0.31
3.20	–	2.97 ± 0.20	1.96 ± 0.35
4.10	–	2.22 ± 0.15	1.62 ± 0.20
4.40 ± 0.20	–	2.22 ± 0.15	1.48 ± 0.30
5.00	–	2.74 ± 0.07	2.09 ± 0.31
7.00	–	2.64 ± 0.05	1.99 ± 0.28
10.00	–	2.63 ± 0.07	2.26 ± 0.10
0.50 ± 0.10	p^-	8.07 ± 0.25	13.49 ± 1.20
0.90 ± 0.20	–	7.38 ± 0.20	6.68 ± 1.30
1.90 ± 0.20	–	4.95 ± 0.15	5.85 ± 0.80
3.20 ± 0.20	–	4.41 ± 0.20	3.82 ± 0.60
4.10 ± 0.20	–	4.23 ± 0.15	2.94 ± 0.30
1.5 10^{-3}	e^-	4.02 ± 0.05	2.60 ± 0.20
2.0 10^{-3}	–	3.66 ± 0.05	2.13 ± 0.20
3.0 10^{-3}	–	3.64 ± 0.05	2.06 ± 0.20
4.0 10^{-3}	–	3.49 ± 0.05	2.86 ± 0.20
5.0 10^{-3}	–	3.23 ± 0.05	2.40 ± 0.20
7.0 10^{-3}	–	3.20 ± 0.05	2.21 ± 0.20
9.0 10^{-3}	–	3.14 ± 0.05	2.42 ± 0.20
11.0 10^{-3}	–	3.02 ± 0.05	2.40 ± 0.20
13.0 10^{-3}	–	3.08 ± 0.05	2.51 ± 0.20
1.36	He^{2+}	21.30 ± 0.10	44.60 ± 1.00
2.00	–	16.34 ± 0.20	26.00 ± 0.50
2.80	–	12.57 ± 0.05	15.90 ± 0.10
4.00	–	9.45 ± 0.05	10.40 ± 0.20
6.00	–	7.08 ± 0.05	6.40 ± 0.10
9.24	–	5.10 ± 0.05	4.90 ± 0.10
12.80	–	4.21 ± 0.10	4.10 ± 0.20
18.00	–	3.63 ± 0.05	3.50 ± 0.20

TABLE 3

$R^{(2)}$ and $R^{(3)}$ for p^+, p^-, e^- and He^{2+} on Ar obtained in this work.

E(MeV)	Projec-tile	$R^{(2)}=\sigma^{2+}/\sigma^{+}$ [10^{-2}]	$R^{(3)}=\sigma^{3+}/\sigma^{+}$ [10^{-3}]
0.10	p^+	14.36 ± 0.10	1.20 ± 0.15
0.50 ± 0.10	–	5.76 ± 0.50	8.90 ± 0.80
1.00	–	4.42 ± 0.26	10.4 ± 0.6
1.20 ± 0.20	–	4.73 ± 0.30	12.4 ± 0.8
1.90	–	4.81 ± 0.15	12.7 ± 0.5
2.00	–	4.42 ± 0.13	12.3 ± 0.3
3.00	–	4.50 ± 0.01	12.8 ± 0.4
3.20	–	4.59 ± 0.15	12.5 ± 0.3
4.10	–	4.59 ± 0.15	13.4 ± 0.8
4.40 ± 0.20	–	4.96 ± 0.20	14.1 ± 0.8
5.00	–	4.72 ± 0.12	13.7 ± 0.5
7.00	–	4.75 ± 0.07	13.8 ± 0.3
10.00	–	4.91 ± 0.13	13.3 ± 0.4
0.50 ± 0.10	p^-	8.10 ± 0.50	9.4 ± 1.0
0.90 ± 0.20	–	6.93 ± 0.30	11.2 ± 1.0
1.90 ± 0.20	–	6.13 ± 0.20	12.5 ± 1.0
3.20 ± 0.20	–	5.22 ± 0.20	12.3 ± 1.0
4.10 ± 0.20	–	5.50 ± 0.15	14.0 ± 0.4
$1.5\ 10^{-3}$	e^-	4.54 ± 0.20	10.68 ± 0.50
$2.0\ 10^{-3}$	–	4.74 ± 0.20	9.79 ± 1.00
$3.0\ 10^{-3}$	–	4.77 ± 0.15	12.91 ± 0.50
$4.0\ 10^{-3}$	–	5.11 ± 0.15	13.88 ± 0.50
$5.0\ 10^{-3}$	–	5.22 ± 0.10	14.24 ± 0.30
$7.0\ 10^{-3}$	–	5.18 ± 0.10	14.24 ± 0.30
$9.0\ 10^{-3}$	–	5.27 ± 0.15	15.13 ± 0.50
$11.0\ 10^{-3}$	–	5.36 ± 0.10	15.58 ± 0.20
$13.0\ 10^{-3}$	–	5.47 ± 0.15	15.31 ± 0.50
1.36	He^{2+}	16.56 ± 0.10	30.30 ± 1.00
2.00	–	12.15 ± 0.10	20.60 ± 1.00
2.80	–	9.98 ± 0.10	19.70 ± 0.20
4.00	–	8.00 ± 0.10	17.50 ± 0.20
6.00	–	6.38 ± 0.10	17.00 ± 0.20
9.24	–	5.57 ± 0.10	15.60 ± 0.30
12.80	–	5.75 ± 0.10	16.00 ± 0.20
18.00	–	5.57 ± 0.15	15.60 ± 0.50

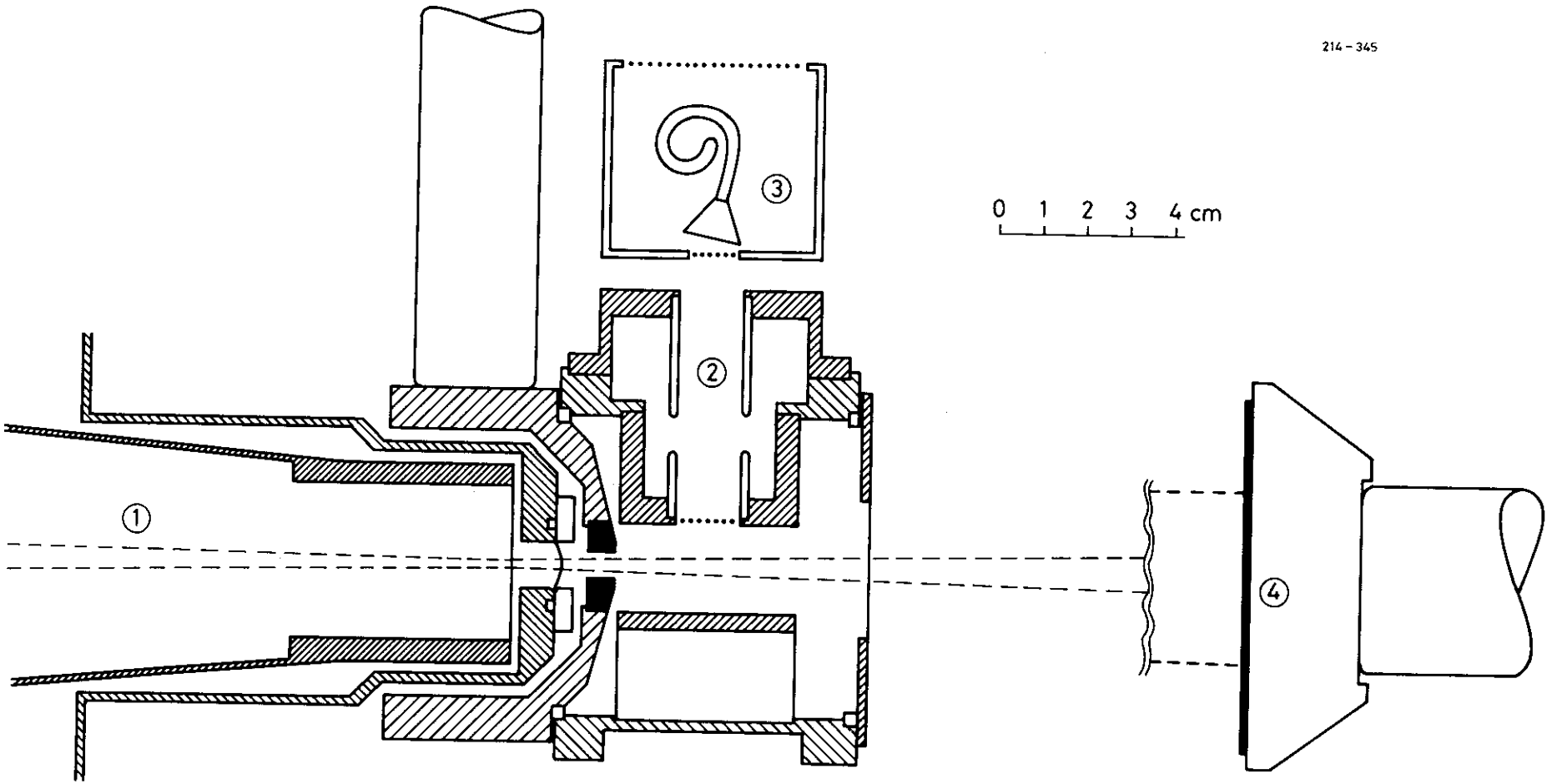

Fig. 1

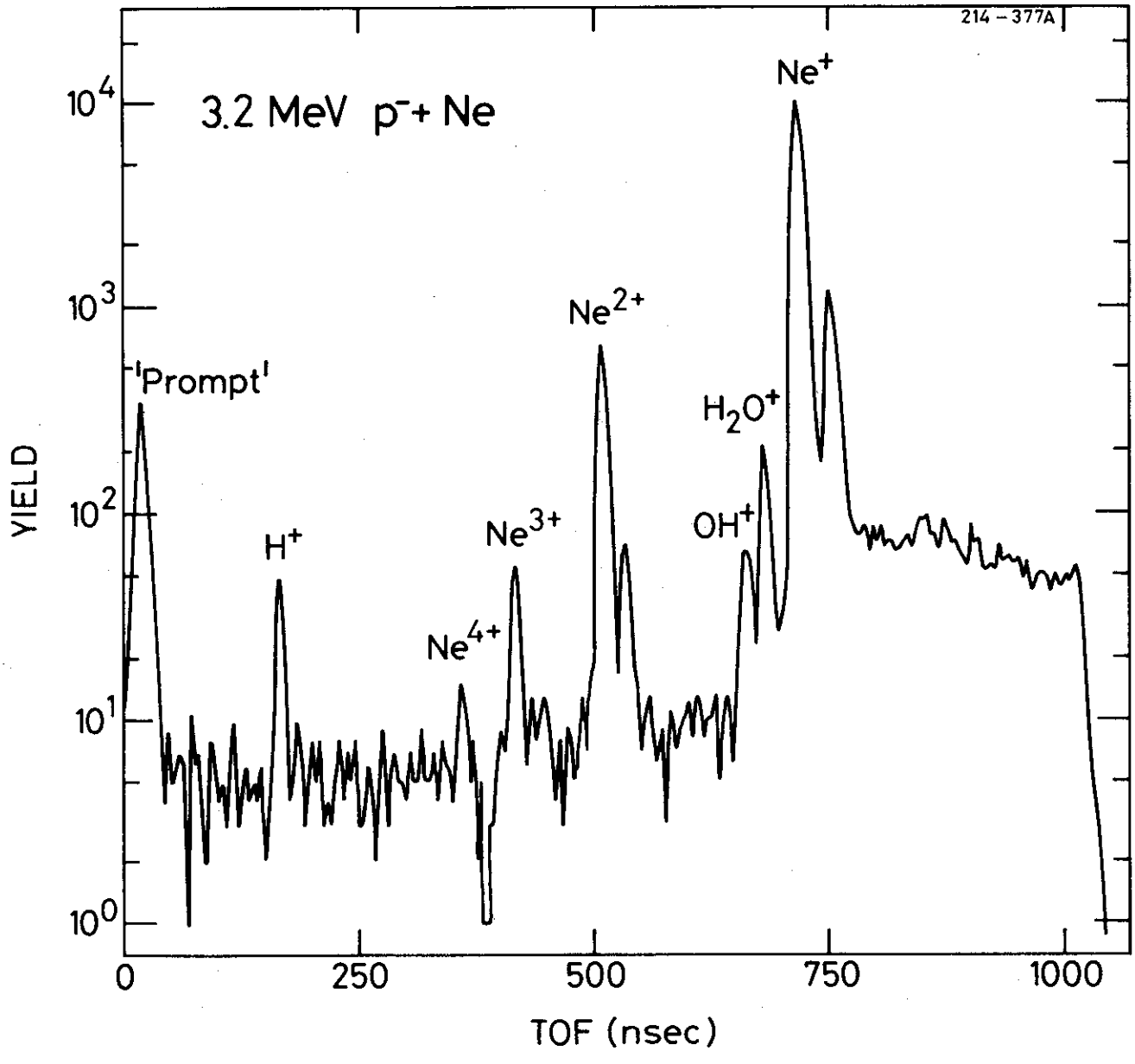
214 – 377A
3.2 MeV p⁻ + Ne
YIELD
TOF (nsec)
'Prompt'
H+
Ne4+
Ne3+
Ne2+
OH+
H2O+
Ne+
10^4
10^3
10^2
10^1
10^0
0
250
500
750
1000

Fig. 2

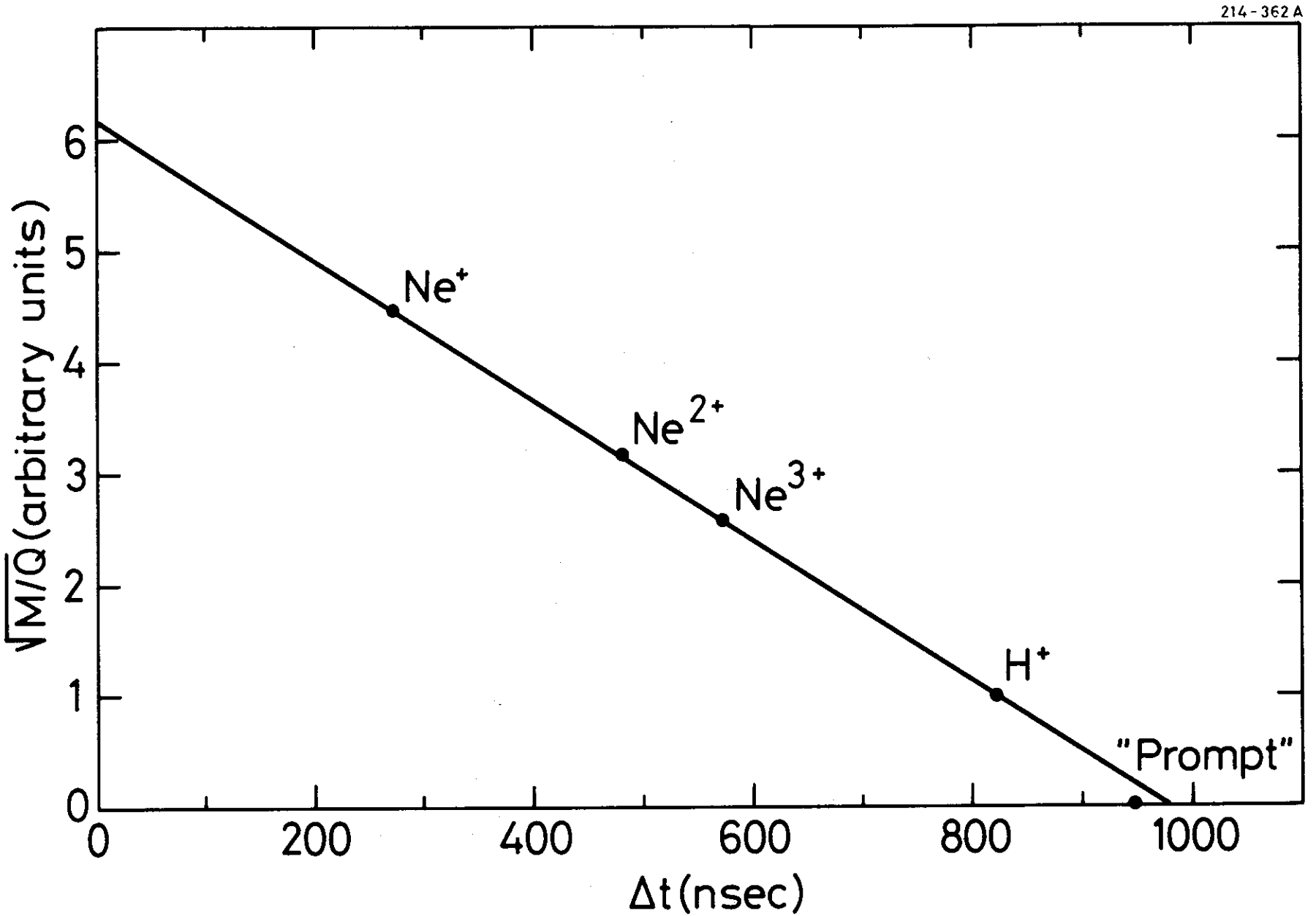
214-362 A
$\sqrt{M/Q}$ (arbitrary units)
0
1
2
3
4
5
6
0
200
400
600
800
1000
Δt (nsec)
Ne+
Ne2+
Ne3+
H+
"Prompt"

Fig. 3

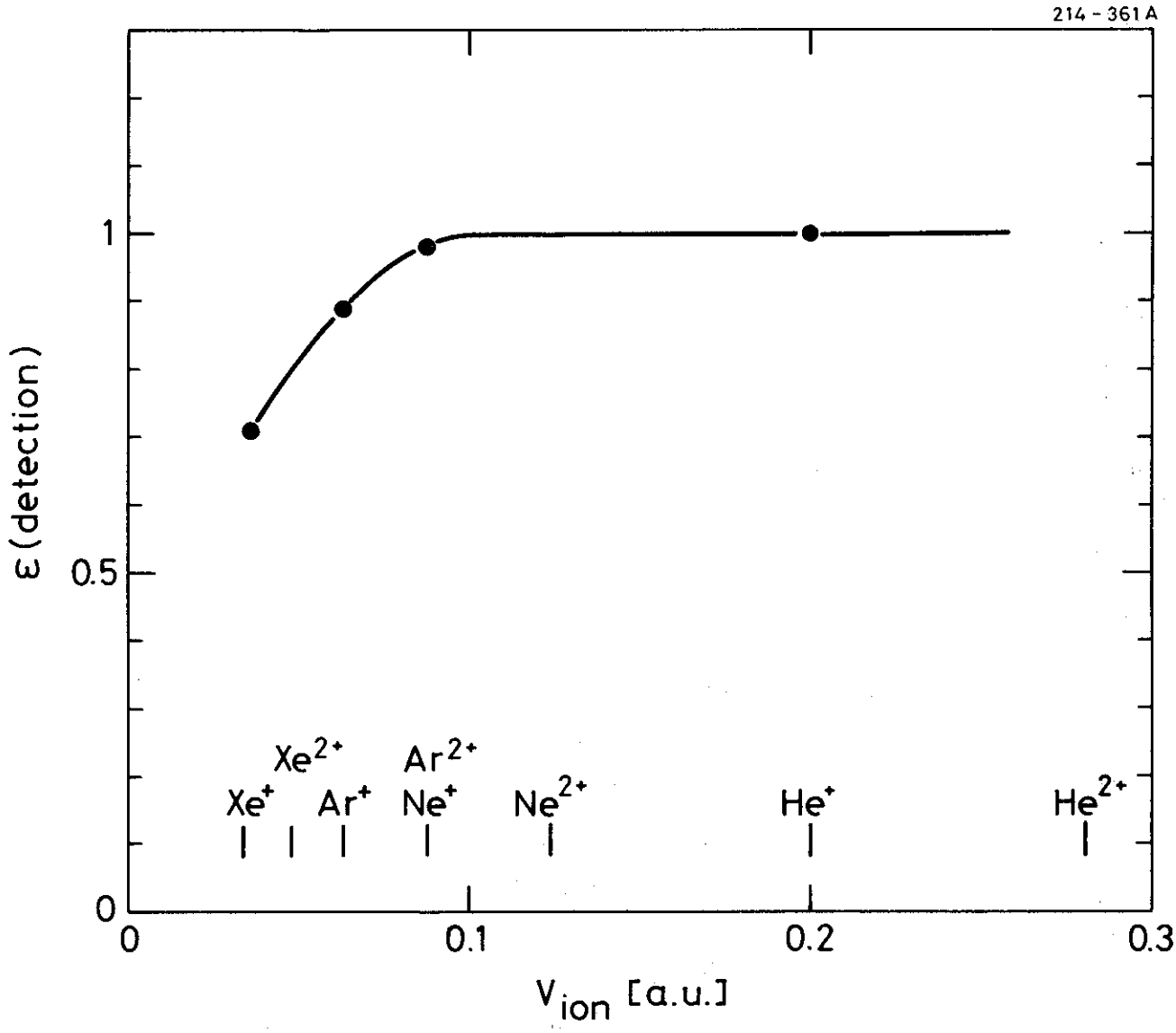
214 - 361 A
ε (detection)
1
0.5
0
0
0.1
0.2
0.3
V ion [a.u.]
Xe+
Xe2+
Ar+
Ar2+
Ne+
Ne2+
He+
He2+

Fig. 4

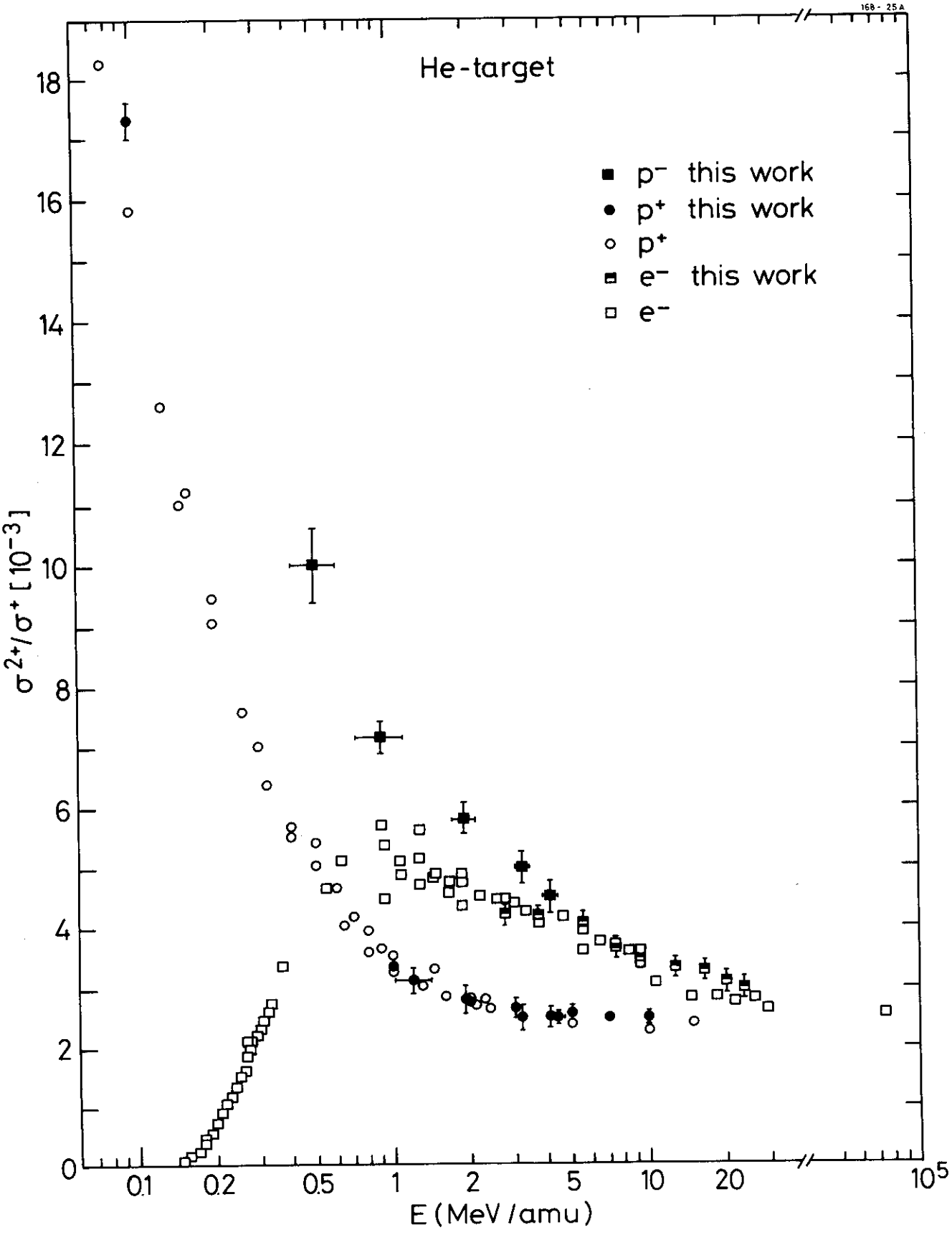
168 - 25 A
He-target
p⁻ this work
p⁺ this work
p⁺
e⁻ this work
e⁻
σ²⁺/σ⁺ [10⁻³]
E (MeV/amu)
0
2
4
6
8
10
12
14
16
18
0.1
0.2
0.5
1
2
5
10
20
10⁵

Fig. 5

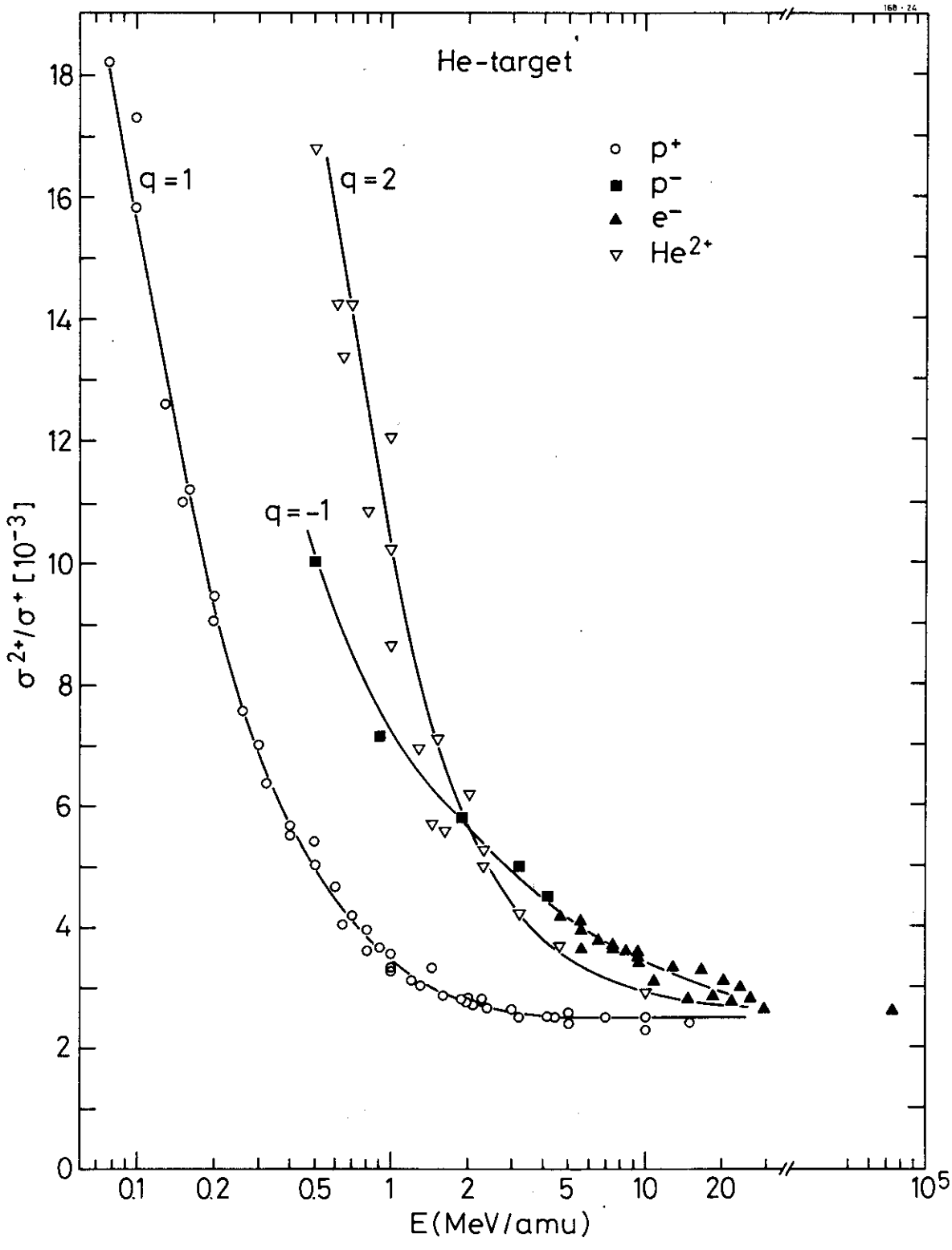
He-target
q = 1
q = 2
q = -1
p+
p−
e−
He2+
σ2+/σ+ [10−3]
E(MeV/amu)
0
2
4
6
8
10
12
14
16
18
0.1
0.2
0.5
1
2
5
10
20
10^5

Fig. 6

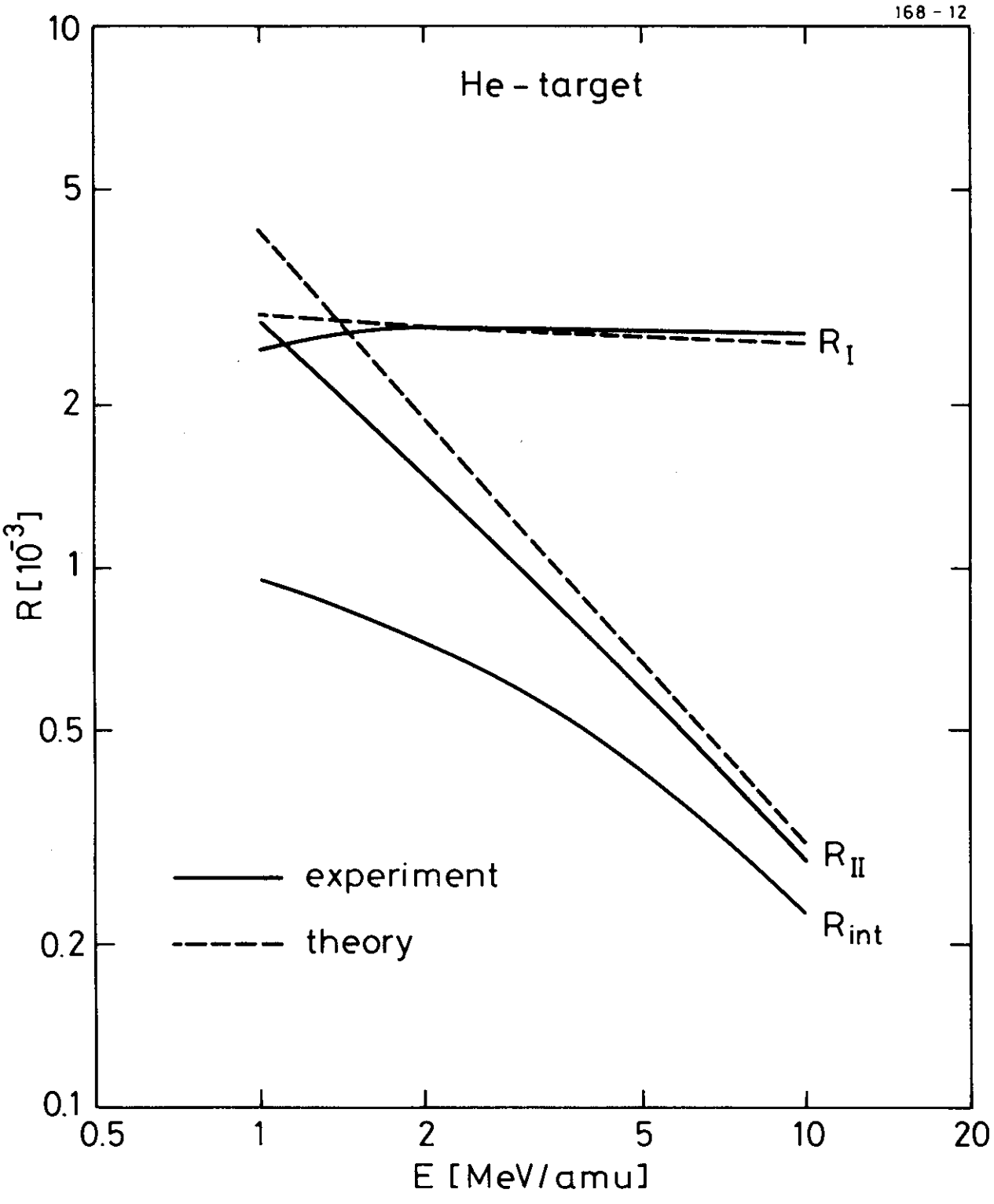
168 - 12
He - target
10
5
2
1
0.5
0.2
0.1
R [10⁻³]
R_I
R_II
R_int
experiment
theory
0.5
1
2
5
10
20
E [MeV/amu]

Fig. 7

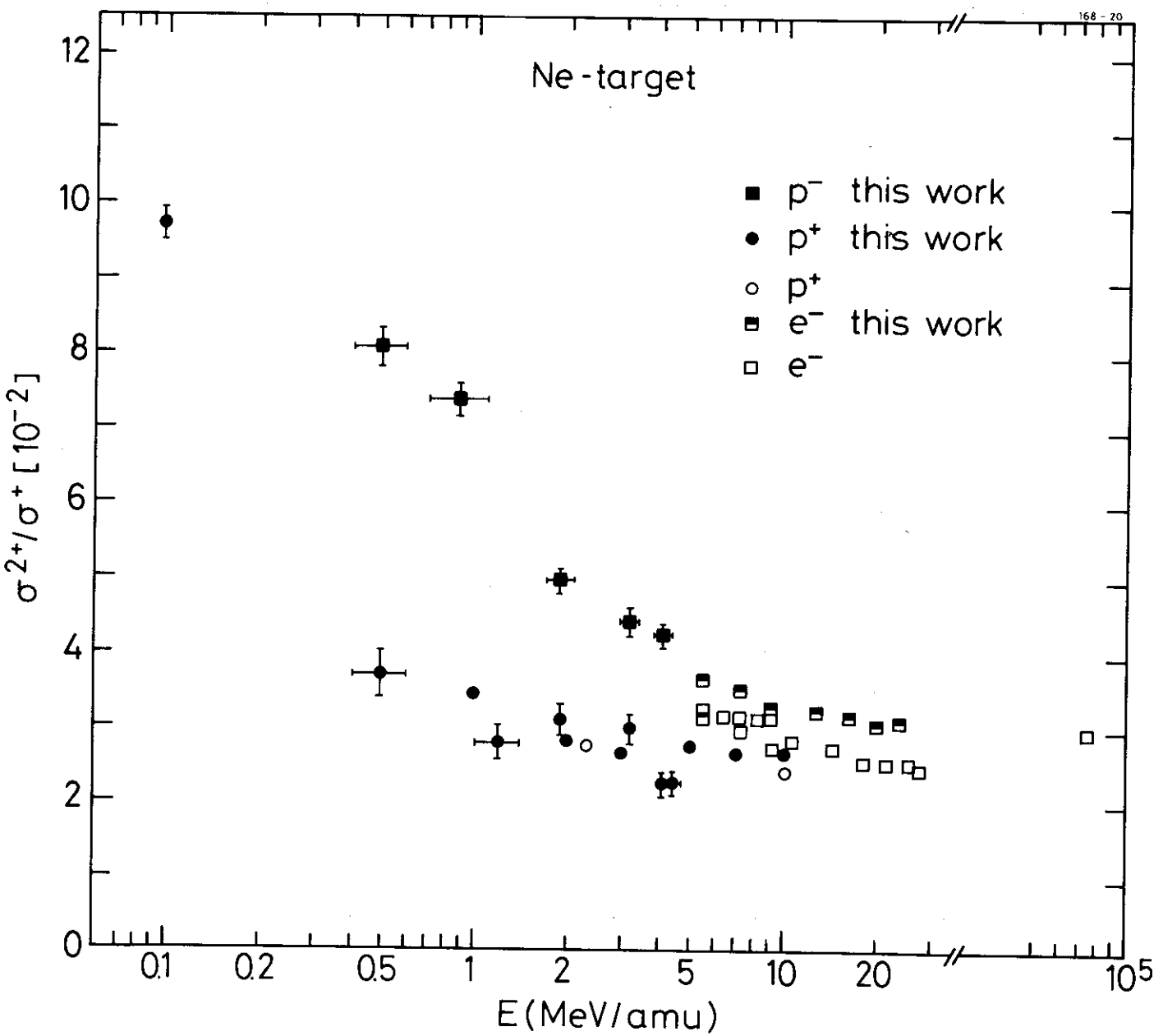
168 - 20
Ne-target
p⁻ this work
p⁺ this work
p⁺
e⁻ this work
e⁻
σ²⁺/σ⁺ [10⁻²]
E (MeV/amu)
0
2
4
6
8
10
12
0.1
0.2
0.5
1
2
5
10
20
10⁵

Fig. 8

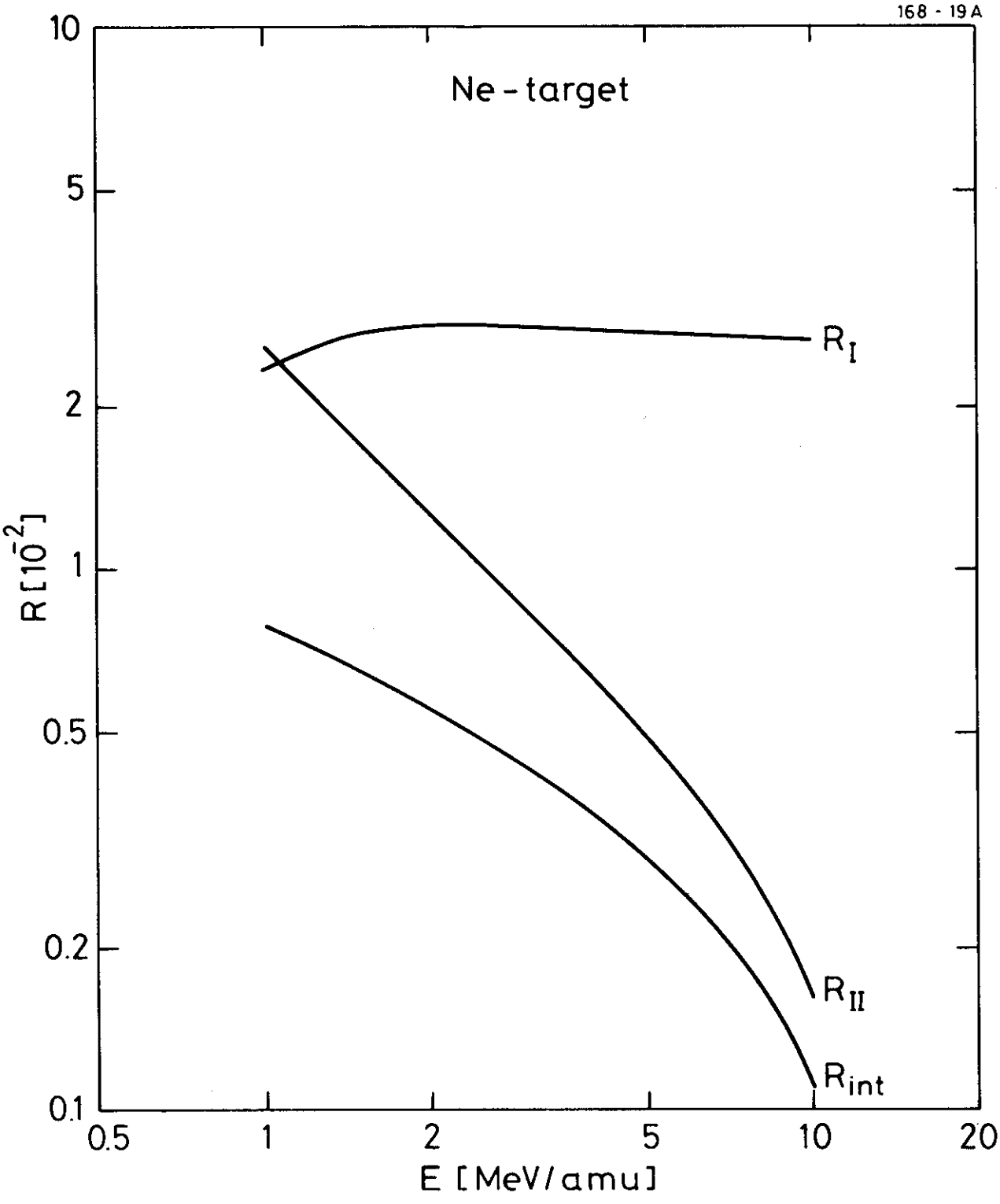
168 - 19A
Ne - target
10
5
2
1
0.5
0.2
0.1
R [10⁻²]
R_I
R_II
R_int
0.5
1
2
5
10
20
E [MeV/amu]

Fig. 9

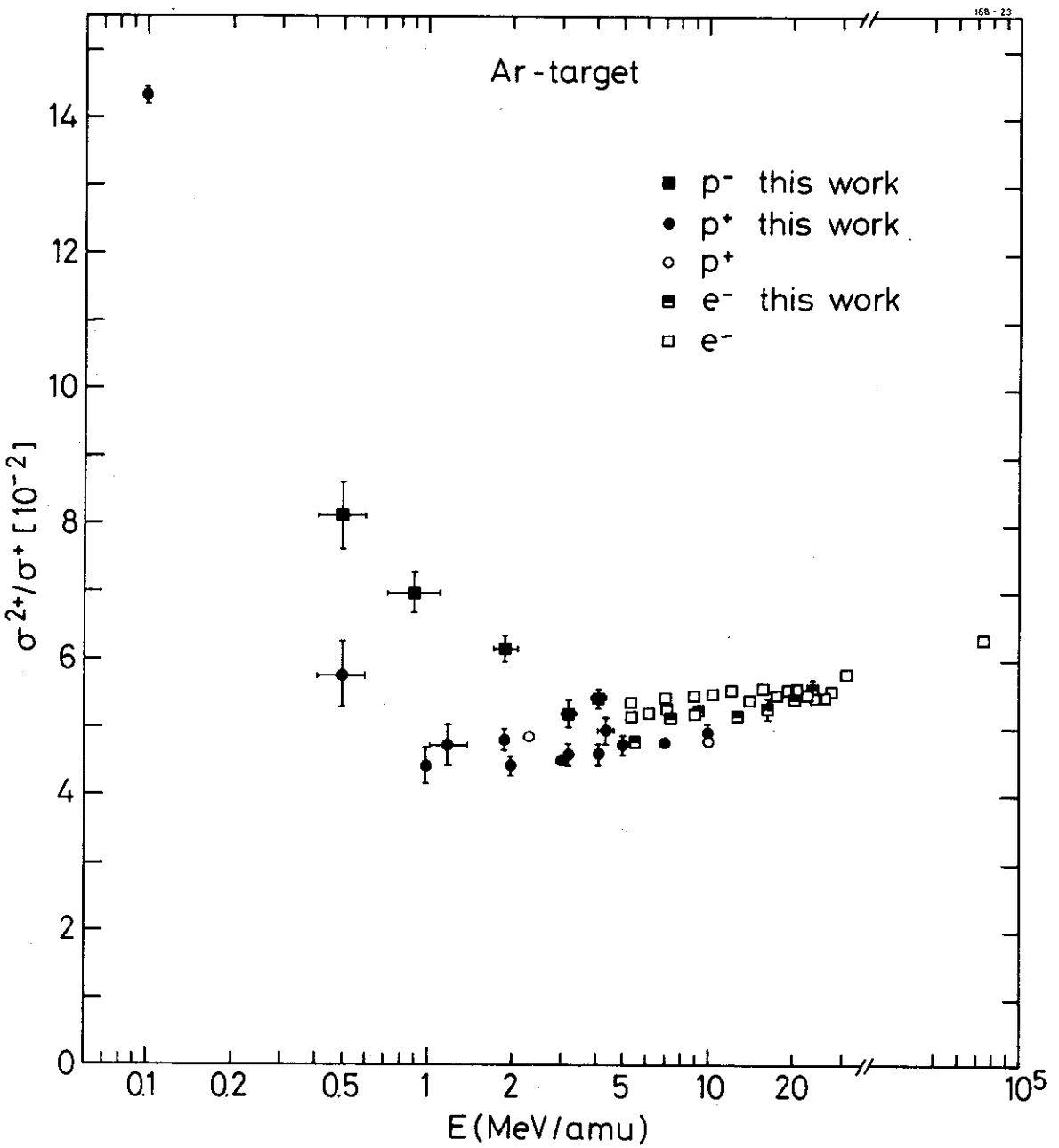
Ar - target
p⁻ this work
p⁺ this work
p⁺
e⁻ this work
e⁻
σ²⁺/σ⁺ [10⁻²]
E (MeV/amu)
0
2
4
6
8
10
12
14
0.1
0.2
0.5
1
2
5
10
20
10⁵

Fig. 10

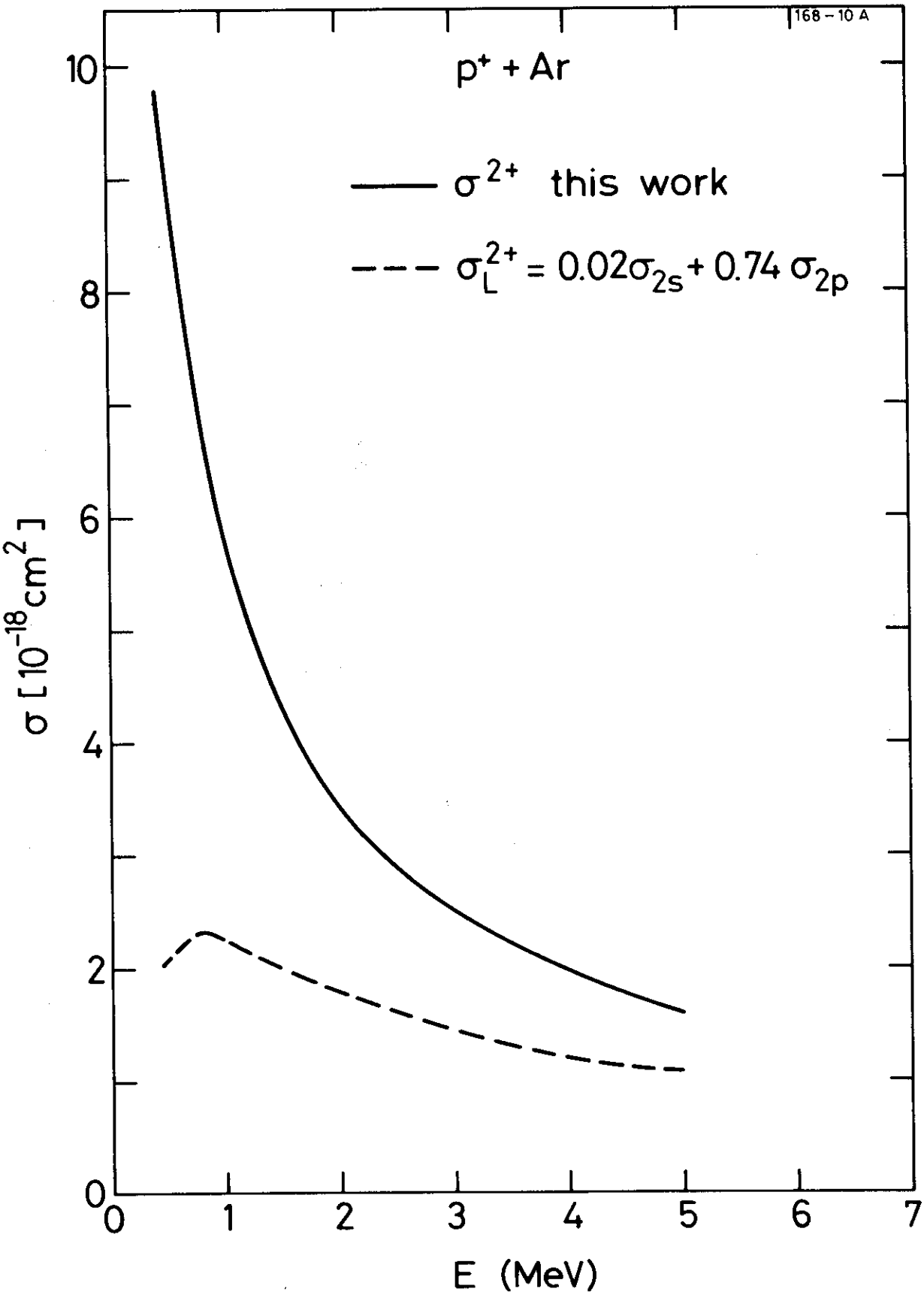
168 - 10 A
p+ + Ar
σ 2+ this work
σ L 2+ = 0.02σ 2s + 0.74 σ 2p
σ [10-18 cm2]
E (MeV)
0
2
4
6
8
10
0
1
2
3
4
5
6
7

Fig. 11

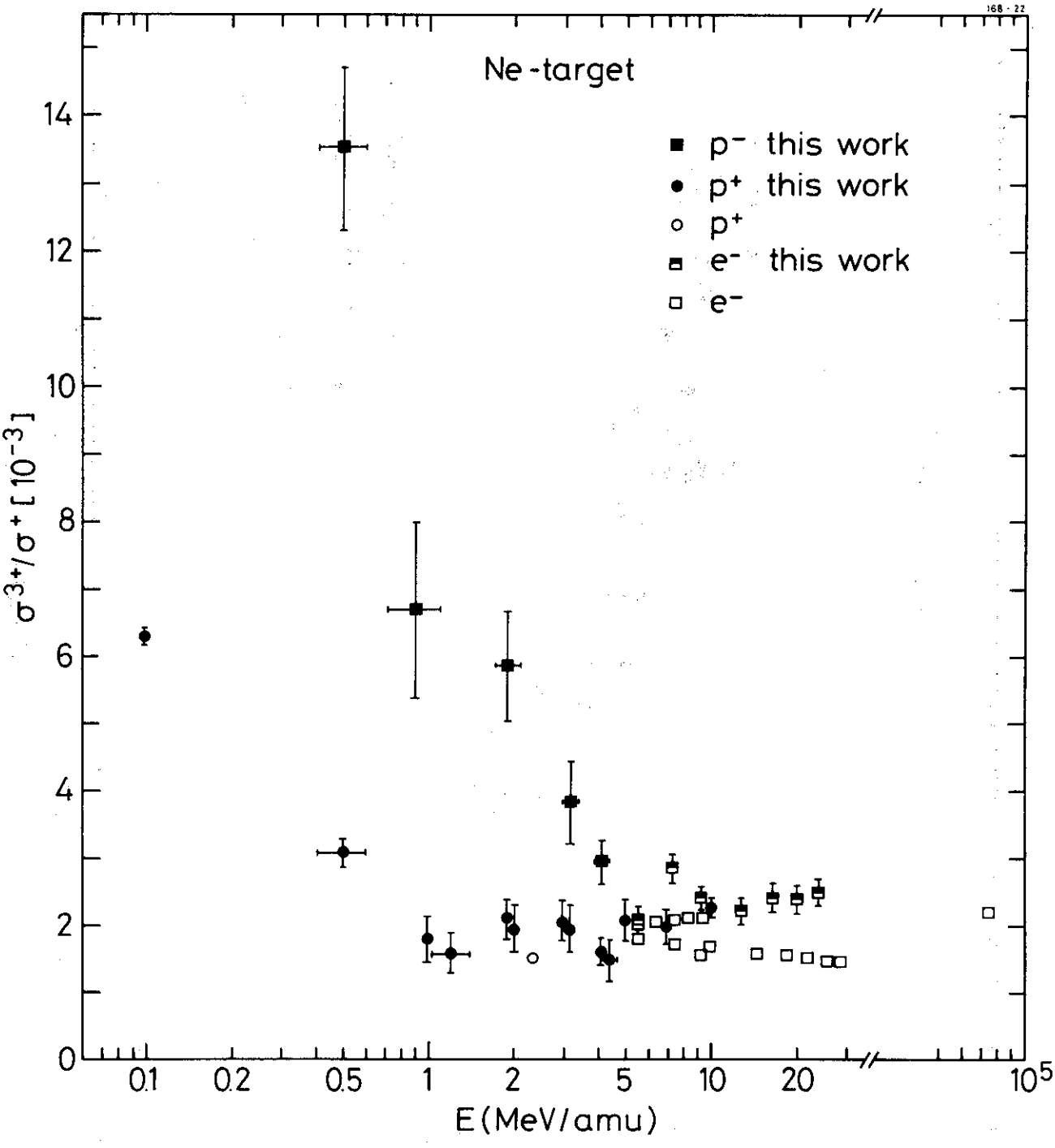
168 - 22
Ne-target
p⁻ this work
p⁺ this work
p⁺
e⁻ this work
e⁻
σ3+/σ+ [10⁻³]
E (MeV/amu)
0
2
4
6
8
10
12
14
0.1
0.2
0.5
1
2
5
10
20
10⁵

Fig. 12

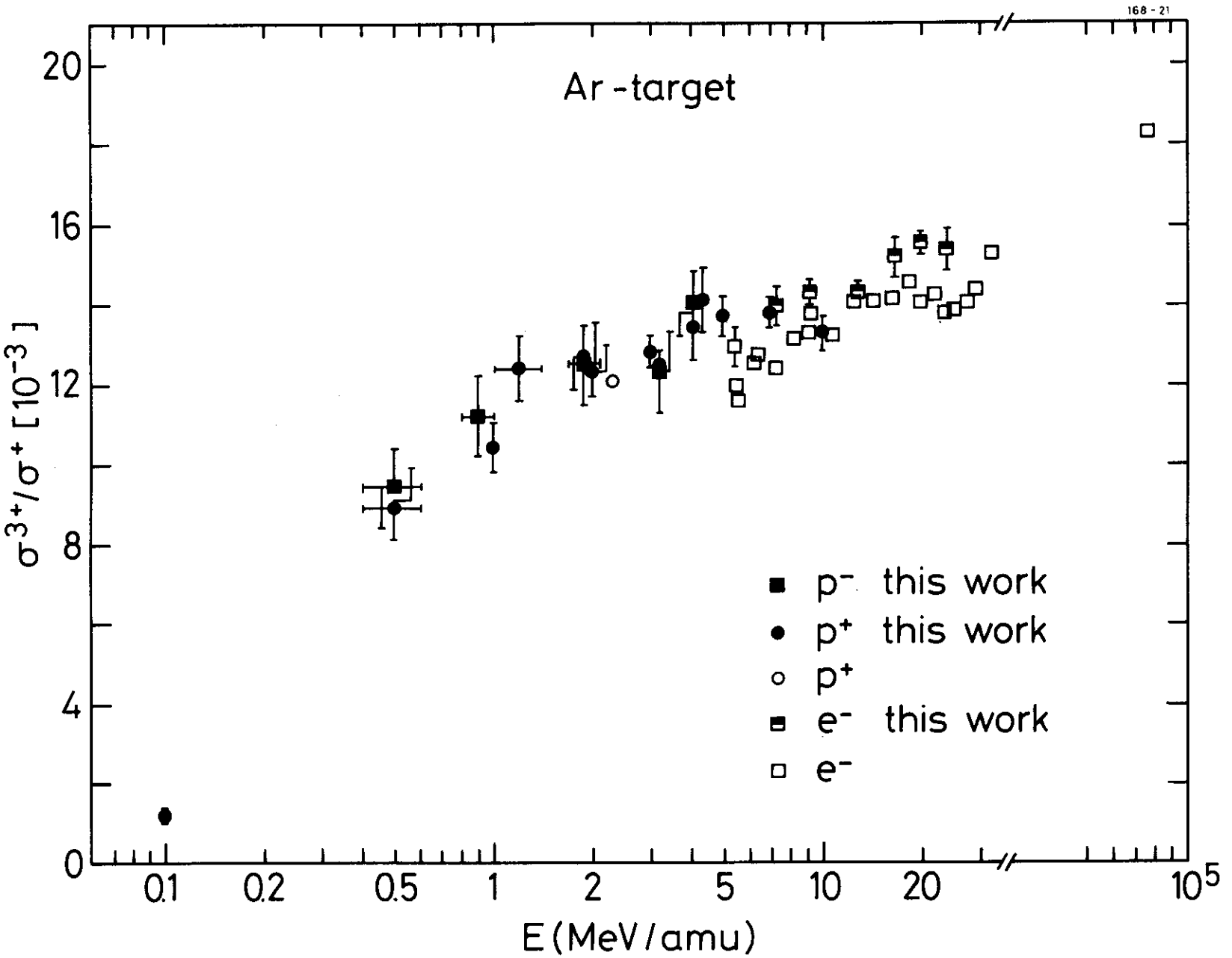
168 - 21
Ar -target
σ^{3+}/σ^{+} [10^{-3}]
E (MeV/amu)
p⁻ this work
p⁺ this work
p⁺
e⁻ this work
e⁻
0
4
8
12
16
20
0.1
0.2
0.5
1
2
5
10
20
10^5

Fig. 13

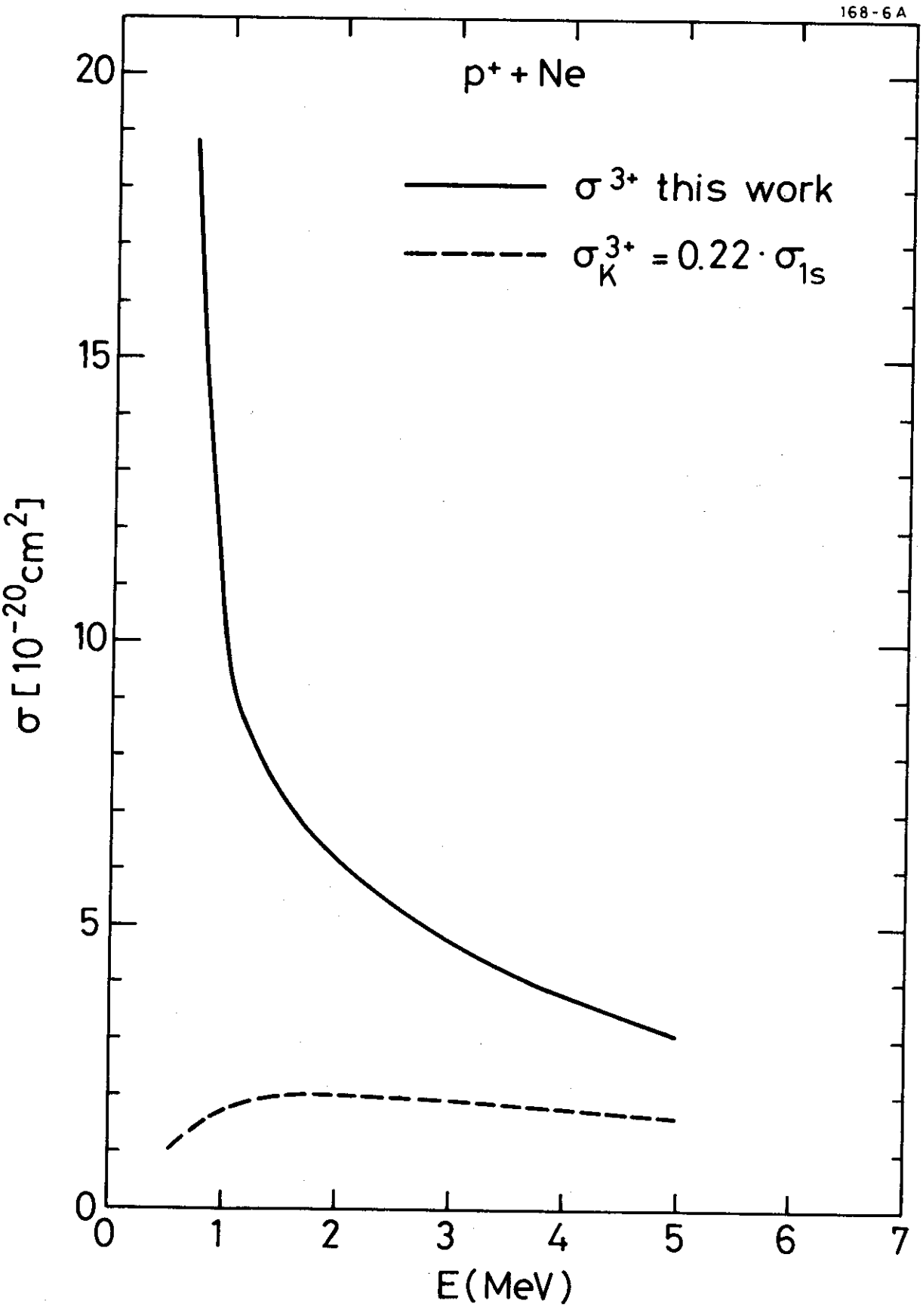
168-6A
p+ + Ne
σ 3+ this work
σ K3+ = 0.22 · σ 1s
σ [10-20cm2]
E(MeV)
0
5
10
15
20
0
1
2
3
4
5
6
7

Fig. 14

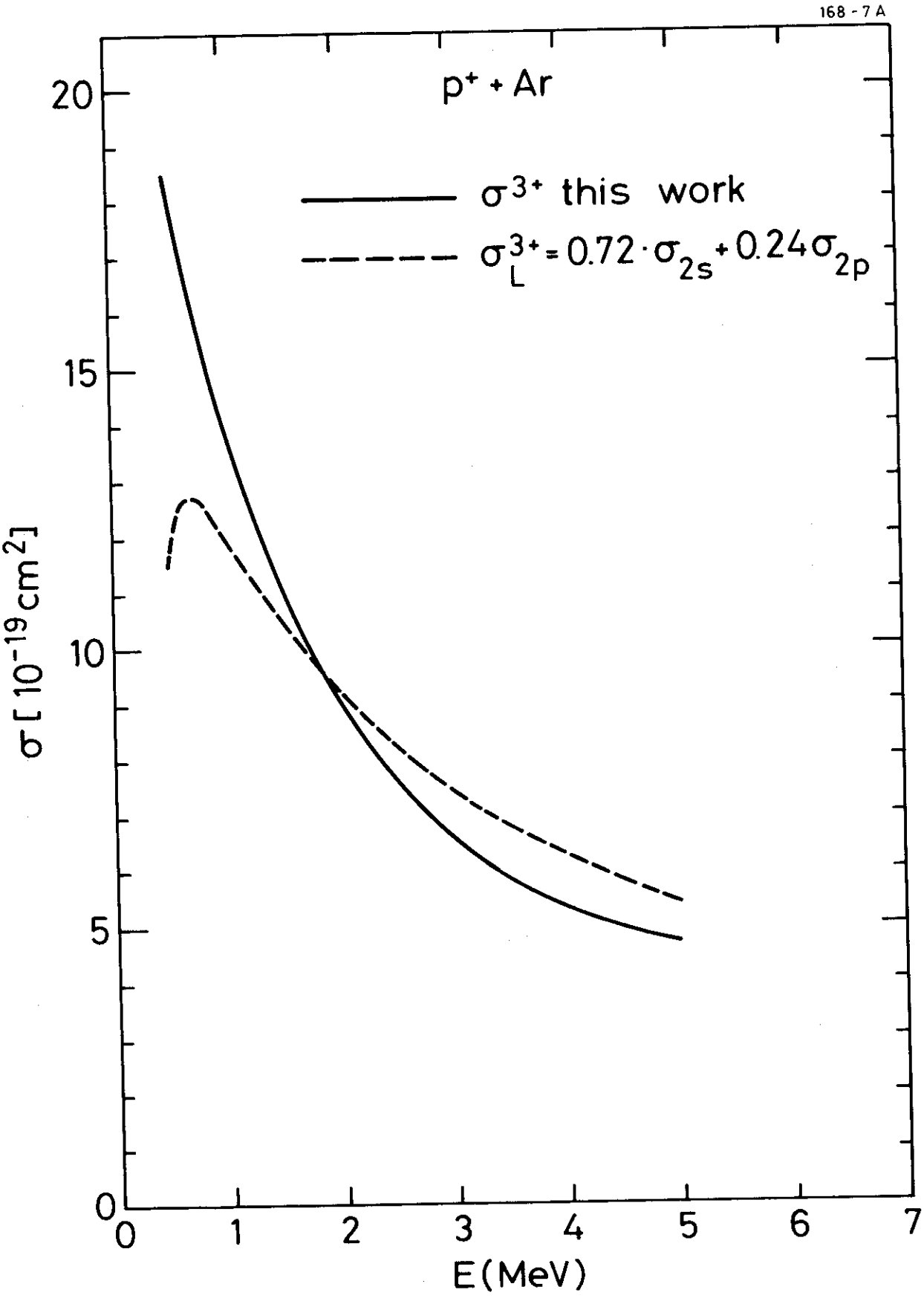
168 - 7 A
p+ + Ar
σ3+ this work
σL3+ = 0.72 · σ2s + 0.24σ2p
σ [10-19 cm2]
E (MeV)
0
5
10
15
20
0
1
2
3
4
5
6
7

Fig. 15